Linear Optical Thin Films Formed by Electrostatic Self-Assembly

by

Zhaoju Luo

Thesis submitted to the Faculty of
Virginia Polytechnic Institute and State University
In partial fulfillment of the requirements for the degree of

Master of Science
in
Electrical Engineering

APPROVED:

Richard O. Claus, Chairman
Bill Spillman
Ira Jacobs

June 9, 2000
Blacksburg, Virginia

Keywords: electrostatic self-assembly (ESA), linear optical thin films, dielectric stack filter, antireflection coating

Linear Optical Thin Films Formed by Electrostatic Self-Assembly

Zhaoju Luo

(ABSTRACT)

The Electrostatic Self-Assembly (ESA) technique possesses great advantages over traditional thin film fabrication methods, making it an excellent choice for a number of applications in the fields of linear and nonlinear optics, electronics, sensing and surface coatings. The feasibility of fabricating linear optical interference filters by ESA methods is demonstrated in this thesis work. Basic single-anion/single-cation ESA films are synthesized and their optical parameters – refractive index and average thickness for individual bilayer – are investigated to provide a basis for the in-depth design of optical filters. High performance dielectric stack filters and narrowband and wideband antireflection coatings are designed using TFCalc simulation software and are fabricated by ESA. Both bulk film sensitivity and layer sensitivity to manufacturing errors are provided. The significant agreement between simulation and experiment demonstrates the strong capability of ESA to precisely control the refractive index and produce excellent thin film filters. The performance of optical thin film filters is largely enhanced compared to the results of previous methods. The experiment results indicate that the ESA process may be used to fabricate optical filters and other optical structures that require precise index profile control.

ACKNOWLEDGEMENTS

First and foremost, I would like to express my sincere and deep gratitude to my advisor, Dr. Rick Claus for his thoughtful guidance, steadily encouragement and support, and consistently generosity and considerateness. Working with him has been the most rewarding experience of my professional life. I would also like to thank all my committee members, Dr. Bill Spillman and Dr. Ira Jacobs, for their valuable suggestions and insights into this research.

Numerous other people at FEORC have assisted me in this research through helpful comments and technical discussions, including Kristie Cooper, Youxiong Wang, Yanjing Liu, Yongqiang Wang, Yaosheng Chen, Fajian Zhang and Weiwei Du. I appreciate their expertise and their company. Thanks Kristie Cooper for the help during thesis writing. Many thanks to Linda Jones and Ann for their kindly help and enthusiasm.

Finally, I would like to thank my husband, Peng, who has always been my side to support and encourage me and provide me useful idea and suggestions to my work.

This work was supported in part by ARO Grant DAAG55-92-1-0101, AFOSR contract F49620-97-C-0047, and Air Force contract F33615-98-C5421.

TABLE OF CONTENTS

Acknowledgements …….. iii
Table of Contents ……. iv
List of Tables and Figures …… vi

Chapter 1 Introduction 1
1.1 Introduction to the Electrostatic Self-Assembly (ESA) process 2
1.2 Motivation and objectives of this thesis 4
1.3 References 6

Chapter 2 ESA Processing and Film Characterization 7
2.1 Materials 8
2.2 Substrates 9
2.3 Multilayer dip processing procedures 10
2.3.1 Drying procedures 11
2.3.2 Dipping time 12
2.4 Characterization techniques 14
2.5 Summary 15
2.6 References 16

Chapter 3 TFCalc Simulation Software 17
3.1 Introduction to TFCalc 18
3.2 Main properties of TFCalc 21
3.2.1 Design optimization 21
3.2.2 Sensitivity analysis 25
3.3 Summary 27
3.4 References 27

Chapter 4 Linear Optical Filters Formed by ESA 28
4.1 Control of refractive index profile in ESA thin films 30
4.2 Dielectric stack filters 34
4.3 Antireflection (AR) coatings 41
4.4 Summary 47
4.5 References 48

Chapter 5 Conclusion 49

LIST OF TABLES AND FIGURES

Table 2-1. Materials used as film components…… 8

Table 2-2. Substrate materials……. 9

Figure 2-1. ESA films on various substrates…… 9

Figure 2-2. ESA procedures for buildup of multilayer assemblies by consecutive adsorption of anionic and cationic polyelectrolytes…….. 11

Figure 2-3. Thickness of Poly R-478/PDDA ESA films……. 12

Figure 2-4. Absorption spectra of 50 bilayer Poly R-478/PDDA ESA films…….. 12

Figure 2-5. Thickness of PDDA/Poly S-119 ESA films with different dipping times…… 13

Figure 2-6. Absorption of 20 bilayers PDDA/Poly S-119 ESA with different dipping times. 13

Table 2-3. Effect of dipping time on film thickness and optical absorption……... 14

Figure 3-1. The flow diagram for thin film design by TFCalc……. 18

Figure 3-2. The interface of TFCalc……. 19

Figure 3-3. Schematic diagram of the physical system model by TFCalc……... 20

Table 3-1. Three design examples with or without optimization…… 23

Table 3-2. Three design examples with optimization…….. 23

Figure 3-4. Simulated reflectance spectra for the different designs with or without optimization…… 24

Figure 3-5. Simulated reflectance spectra for the different designs with optimization…… 24

Figure 3-6. Film sensitivity to the thickness error of ±5nm for B.3……. 26

Figure 3-7. Film sensitivity to the relative index of ±0.3% for B.3…….. 26

Figure 3-8. Layer sensitivity for B.3……. 27

Figure 4-1. A single thin film…… 29

Table 4-1. Refractive index and thickness for 50-bilayer ESA films…….. 31

Figure 4-2. UV/vis absorbance of Direct Red 75 / PDDA ESA thin films……... 31

Figure 4-3. Film thickness with increasing numbers of bilayers…….. 31

Figure 4-4. Wavelength and thickness dependent refractive index (Left: PDDA / PSS; Right: Poly S-119 / PDDA)…….. 32

Figure 4-5. Process of the self-assembly of 33:67 mixture (XYY multilayer) ESA thin films……... 33

Figure 4-6. UV/vis spectra for increasing X:Y [(PDDA /Direct Red 75):(PDDA/PSS)] ratios in 50-bilayer films……... 33
Figure 4-7. Bulk refractive index vs. percentage of PDDA /Direct Red 75……. 33
Figure 4-8. Quarter-wave stack…… 34
Figure 4-9. Theoretical reflectance spectra for multilayer stacks of alternating λ/4 layers of n_H=2.3 and n_L=1.38 on glass (n_S=1.52) as a function of phase thickness (2πnd/λ). The number of layers is indicated……. 36
Figure 4-10. (a) Dielectric stack filter (b) Refractive index profile…….. 36
Table 4-2. Structure of dielectric stack filter…….. 37
Figure 4-11. Reflectance peak value for dielectric stack filter. The difference between simulation and experiment is indicated for each layer……. 37
Figure 4-12. Dielectric stack filter simulated reflectance spectrum for increasing numbers of λ/4 layer…… 38
Figure 4-13. Dieletric stack filter experimental reflectance spectrum for increasing numbers of λ/4 layer…… 38
Figure 4-14. Calculated sensitivity to the absolute variable thickness ±5nm for 7 layer stack…… 39
Figure 4-15. Calculated sensitivity to the relative variable index ±0.2% for 7 layer stack…. 39
Table 4-3. Peak reflectance comparison between previous and current design…… 40
Table 4-4. Layer structure of narrowband AR filter…….. 42
Table 4-5. Layer structure of wideband AR filter……. 42
Figure 4-16. Simulated reflectance spectrum of narrowband AR filter……... 43
Figure 4-17. Experimental reflectance spectrum of narrowband AR filter…….. 43
Figure 4-18. Simulated reflectance spectrum of wideband AR filter……... 44
Figure 4-19. Measured reflectance spectrum of wideband AR filter…… 44
Figure 4-20. Layer sensitivity for the wideband AR filter…… 45
Table 4-6. Layer structure of wideband AR filter with variable index material…… 45
Figure 4-21. Simulated reflectance spectrum of wideband AR filter with variable index material……... 46
Figure 4-22. Measured reflectance spectrum of wideband AR filter with variable index material……... 46

Chapter 1 *Introduction*

Organic thin films with specific structures and properties have attracted a great deal of interest in recent years due to their potential application in a number of different fields, including linear and nonlinear optics, electronics, sensing and surface coatings [1,2]. These well-ordered films, consisting of molecules with special properties, are carefully aligned between individual layers and the substrate, possessing high stability to thermal change and chemical environments.

The incorporation of molecules into thin films can be achieved spontaneously by molecular self-assembly, without external intervention, so that stable structures are produced at a thermodynamic minimum. The driving forces between the molecules are the chemistry of the intermolecular interactions, e.g. ionic, hydrogen, van der Waals, and covalent bonds [2,3]. Since the molecules adjust themselves to the thermodynamic minimum, defects are limited and self-healing. The resulting structures are stabilized by the interactions between anionic and cationic molecules, and are therefore intrinsically resistant to impurity incorporation. Individual layers within the film may contain different molecules of application-appropriate functionality, allowing the incorporation of multiple functions within a single structure.

A number of self-assembly methods have been used for such film fabrication, such as Langmuir-Blodgett (L-B) films and covalently self-assembled monolayers. A new method of organizing thin films using layer-by-layer adsorption of polyelectrolytes was developed by Decher and co-workers in the 1990s [4,5]. Alternate adsorption of polyanionic and polycationic molecules on oppositely charged surfaces is accomplished by immersion in aqueous polyelectrolyte solutions. This electrostatic self-assembly (ESA) technique offers several advantages, including the ease of fabrication, the availability of numerous water-soluble polyions, and the capability for uniform

and stable multilayer synthesis. A wide variety of molecules, including nonlinear optical chromophores, conducting polymers, biological macromolecules, magnetic materials, dielectrics, and metallic or metallic oxide nanoparticles, can be incorporated into the film to achieve specific functionality. This makes ESA thin films widely used in a number of different fields, including optics, electronics, biosensing and surface modification. The composition and structure of each layer can be controlled by appropriately choosing molecules and adjusting the deposition parameters.

This thesis work extends that of previous researchers concerning potential optical applications of ESA films. Based on the theoretical analysis of linear optical filters with the help of TFCalc simulation software, highly improved performance is achieved after synthesizing and fabricating optical interference filters by ESA with nanoscale control of the refractive index profiles.

This chapter introduces the ESA process and outlines its development and application up to the present, and presents the motivation and objective for this research.

1.1 Introduction to the Electrostatic Self-Assembly (ESA) Process

The concept of the alternate adsorption of oppositely charged polyions began with Iler's [4] demonstration of sequential deposition of negative silica colloids and positive alumina fibrils in 1966. But this novel process was not largely developed until the early 1990s, when Decher and coworkers, at Gutenberg University in Germany, fabricated optically transparent multilayer films of four different polyelectrolytes [5,6]. Uniform growth was verified using UV/vis spectroscopy and small angle X-ray scattering (SAXS). It demonstrated that a periodic structure can be self assembled, with no substrate size limitation, with significant advantages over the L-B method. In-depth research has moved in two important directions: a) the understanding of the process itself and the investigation of variables that control the film structures and b) the incorporation of a wider range of molecules for a number of potential applications in different fields. Decher's group has focused on investigations of process and structure. Other groups have worked on electronic and optical applications of ESA films. Rubner's group at MIT produced band-gap

modulated thin film architectures by assembling electroactive and conductive polyions. More recently, ESA has been used to deposit functional coatings, such as LEDs, magnetics, piezo, hard coatings, biosensors, humidity sensing, and linear and nonlinear optical thin films at the Fiber & Electro-Optic Research Center here at Virginia Tech [7-10].

The basic concept behind the ESA process is simple. A monolayer polycation/polyanion film is assembled on the oppositively charged substrate through the ionic bond. After rinsing in ultrapure water three or four times to remove the loosely adsorbed molecules, the substrate is then immersed in the polyanionic/polycationic solution to adsorb a molecular monolayer. The substrate is rinsed again in ultrapure water to remove the loose molecules. Thus one bilayer (polycation-polyanion) is synthesized. Repeating this self-assembly dipping process results in multilayer films.

ESA processing of optical thin films for linear and nonlinear applications has the following major advantages over traditional methods [10].

- **Excellent nanoscale molecular level uniformity** permits the fabrication of high quality films and devices with extremely low scattering losses.
- **Capability for high quality, multilayer fabrication** is allowed due to the uniformity of each layer and the avoidance of geometrical defects caused by conventional covalent bonding-based self-assembled monolayer (SAM) approaches. Multilayer structures allow the incorporation of multiple functions into a single film.
- **Broad range of layer functionality** - Since the ESA technique involves the use of alternating anionic and cationic layers, materials that provide enhanced secondary properties can be easily incorporated, allowing control of the optical, electronic, magnetic, thermal and mechanical properties.
- **Compatibility with conventional photolithographic processes** - Multiple layers self-assembled by ionic bonding may be patterned using standard methods to create integrated devices.
- **Long-term stability** - The molecules arrange themselves to achieve a thermodynamic minimum; the structural ordering of the self-assembled film will not decay over time.

- **Excellent long-term environmental robustness** is achieved by excellent molecular order that limits defects, and can be enhanced through the incorporation of pliable high performance polymers (such as polyimides and polyamides).
- **Synthesis at room temperature and pressure** - Avoiding high temperature processes allows multilayer coatings to be created on nearly any solid substrate, including plastics, semiconductors, organic films, ceramics or metals, without degrading or destroying the substrate.
- **Low-cost manufacturing** - ESA thin-film fabrication simply consists of dipping or spraying a charged substrate with alternate aqueous polyelectrolyte solution and rinsing it. Capital equipment costs for basic fabrication are thus extremely low, and the process may be upscaled in size and volume and easily automated.
- **Environmentally friendly** - ESA is a water-based process, involving no volatile organic compounds, and consuming negligible power.
- **Independent of substrate size or topology** - In contrast to Langmuir-Blodgett films, substrates of any size or shape may be coated uniformly on all surfaces.

1.2 Motivation and objectives of this thesis

New thin-film materials and devices with specific optical, electronic, mechanical and other properties are required for applications in communication systems, information storage, display systems, sensors, and other fields. ESA makes itself an excellent choice in these applications due to its strong capability to incorporate multiple properties into the films at the molecular level and the desire for fast and inexpensive production.

Conventional thin film methods fall short of meeting these requirements [10]. For example, spin coating lacks control of exact thickness and molecular-level structure in spite of being inexpensive. Vapor deposition technique produces thermal stress, which reduces film integrity in micron-thick films. For L-B films, little flexibility exists in choosing molecules of different structures and functions as well as substrates shape and size. Also it is very difficult to form films several hundred Ångstroms thick of good optical quality and the resulting films are not

stable to thermal or chemical treatment. The limitation of covalent self-assembly is that the surface defects must be repaired by cross-linking or they will grow exponentially, and each layer may require several chemical activation steps; the synthesis of multilayer films can be very time consuming.

As indicated in Section 1.1, ESA offers a number of advantages over these methods. Due to the layer-by-layer nature of ESA, a variety of polyions can be used as long as proper polyanion/polycation alternation is maintained, allowing the incorporation of a wide variety of molecules to provide multiple functions and properties. Its application has already been demonstrated in work related to LEDs, magnetics, hard coatings, biosensors, linear and nonlinear optical thin films.

The major objective of this thesis is to design and fabricate high performance linear optical thin film components, especially dielectric stack filters and antireflection (AR) coatings. The following tasks are included.

- Theoretical design and optimization of the structure of linear optical filters using TFCalc simulation software, including sensitivity analysis
- Demonstration of multimicron-thick films with controlled refractive index profiles
- Synthesis of prototype thin films, filters and coatings, with optical properties designed at the molecular level
- Comparison of the results between experiment and theory

This thesis is organized as follows. Chapter 2 presents a discussion of ESA processing and film characterization methods. The origin of materials and substrates used are given. Some process variables that control film properties are investigated. Chapter 3 introduces the simulation software – TFCalc. The primary properties and advantages of TFCalc, including design optimization and sensitivity analysis, are presented. The application of ESA technology to linear optical interference filters is discussed in Chapter 4. Basic ABAB layered ESA films of multiple material combinations are fabricated and characterized. High performance dielectric stack reflectance filters and antireflection (AR) filters are designed and optimized by using TFCalc and

fabricated by ESA. The good agreement between experiment and theory is shown. Chapter 5 gives a summary of the significance and primary contributions of this thesis work. Recommendations for future research in this area are made.

1.3 References

1. D. Li and O. Ramos Jr., "Molecular Self-Assemblies as Advanced Materials", in *Photonic Polymer Systems - Fundamentals, Methods and Applications*, Marcel Dekker, New York (1998).
2. H. Fuchs, H. Ohst and W. Prass, "Ultrathin Organic Films: Molecular Architectures for Advanced Optical, Electronic and Bio-Related Systems", *Adv. Mater.* 3, no.1, 10 (1991).
3. Y. Lvov, G. Decher and H. M. hwald, "Assembly, Structural Characterization, and Thermal Behavior of Layer-by-Layer Deposited Ultrathin Films of Poly(vinyl sulfate) and Poly (allylamine)," Langmuir 9, 481 (1993).
4. G. Decher, J.D. Hong and J. Schmitt, "Buildup of ultrathin multilayer films by a self-assembly process: II. Consecutively alternating adsorption of anionic and cationic polyelectrolytes on charged surfaces", *Thin Solid Films* 210/211, 831 (1992).
5. J.D. Hong, et al, "Layer-by-layer deposited multilayer assemblies of polyelectrolytes and proteins: from ultrathin films to protein arrays", *Progr. Colloid Polym. Sci.* 93, 98 (1993).
6. K.H. Guenther, *Thin Films for Optical Systems*, *SPIE* Vol. 1782, Bellingham, Wash. (1993)
7. Y. Liu, A. Wang and R. Claus, "Molecular Self-Assembly of TiO_2/Polymer Nanocomposite Films", *J. Phys. Chem. B* 101, 1385 (1997).
8. Y. Liu, A. Wang and R. Claus, "Layer-by-layer electrostatic self-assembly of nanoscale Fe_3O_4 particles and polyimide precursor on silicon and silica surfaces", *Appl. Phys. Lett.* 71, October 1997.
9. F.J. Arregui et al., "Optical Fiber Humidity Sensor Formed by the Ionic Self-Assembly Monolayer Process", *Proc. SPIE 3670*, Newport Beach, CA, March 1999.
10. K. Cooper, "Electrostatic Self-Assembly of Linear and Nonlinear Optical Thin Films", Ph.D. dissertation, Electrical Engineering Department, Virginia Polytechnic Institute & State University, Blacksburg, Virginia, May 1996.

Chapter 2 *ESA Processing and Film Characterization*

Electrostatic self-assembly processes offer significant advantages over traditional methods of thin film synthesis [1,2]. Most importantly, the ionic bonding of molecules allows extremely uniform films to be deposited on substrates of arbitrary size and shape, permitting nanoscale control over the film thickness and refractive index. In addition, ESA synthesis is performed at room temperature and pressure, which enables the ESA process to apply coatings to almost any substrate material, including ceramics, plastics, metals, semiconductors or organic materials. The incorporation of a wide range of inorganic and organic molecules allows the molecular-level control of coating electronic, conductive, optical, magnetic, thermal and mechanical properties. The resistance of the thin films to chemical and environmental effects is highly improved by ESA processings. Finally, the ESA process does not require large equipment; only a pure water system is needed. Equipment costs are therefore low and the process can easily be upscaled and automated.

This chapter discusses the ESA processes used in detail. The chapter is organized as follows. The first section explains the materials used in film fabrication and characterization. Section 2.2 shows the capability of ESA processing to coat substrates of a wide variety of materials, shapes and sizes. Processing procedures that can control the resulting film characteristics are discussed in Section 2.3. Section 2.4 presents techniques for thin film characterization. Finally, the chapter summary is given in Section 2.5.

2.1 Materials

Numerous materials were required for this research, as both film components and substrates. Tables 2-1 shows the materials used as film components. Substrates materials are discussed in the next section. All materials were used without further purification. Solutions are made by dissolving the polymers in acidic solutions for all the film materials, with special density and pH values.

The ultrapure water used for all ESA procedures was obtained from a Barnstead Nanopure III system, and had a resistivity greater than 17 MΩ•cm.

Table 2-1. Materials used as film components.

MOLECULE	DETAILS	MANUFACTURER
PDDA	Poly diallyldimethyl ammonium chloride 20 wt.% in H_2O M_w 400,000-500,000	Aldrich
PAH	Poly allylamine hydrochloride M_n 50,000-65,000	Aldrich
PSS	Poly(sodium 4-styrenesulfonate) M_w ca. 70,000	Aldrich
Poly S-119	M_w 100,000-160,000 Poly(vinylamine) backbone Azo chromophore Color: orange Poly S-119 is a trademark of Dynapol, Palo Alto, CA	Sigma
Direct Red 75	Molecular Formula: $C_{33}H_{26}N_8O_{15}S_4$ Molecular Weight: 990.8 UV wavelength max. (nm): 522 Dye content ~30%	Aldrich
Direct Yellow 50	Molecular Formula: $C_{35}H_{28}N_6O_{13}S_4$ Molecular Weight: 956.83 UV wavelength max. (nm): 390 Dye content ~40%	Aldrich
ZrO_2 nanocluster	F. W. 23.22 20 wt.% in H_2O; colloidal dispersion	Alfa Aesar
PCBS	Poly{1-[4-(3-carboxy-4-hydroxyphenylazo)-benzenesulfonamido]-1,2-ethanediyl, sodium salt}	Aldrich

2.2 Substrate

Table 2-2 shows different substrate materials.

Table 2-2. Substrate materials.

MATERIAL	MANUFACTURER
Quartz	Chemglass, Inc.
Single crystal silicon	EL-CAT, Inc.
Glass microscope slides	Fisher Scientific
Indium tin oxide (ITO) -coated glass	Applied Films, Inc.

Previous and current experiments show that ESA processing can be applied to multiple substrates of arbitrary size, shape and material [2]. Uniform ESA films have been dipped on flat, curved, and geometrically complicated substrates with different sizes. Substrates made of various materials, including glass, quartz, single-crystal silicon, plastic and transparent conductive substrates, were used in the experiments. Figure 2-1 shows some kinds of substrates with different size, shape and materials.

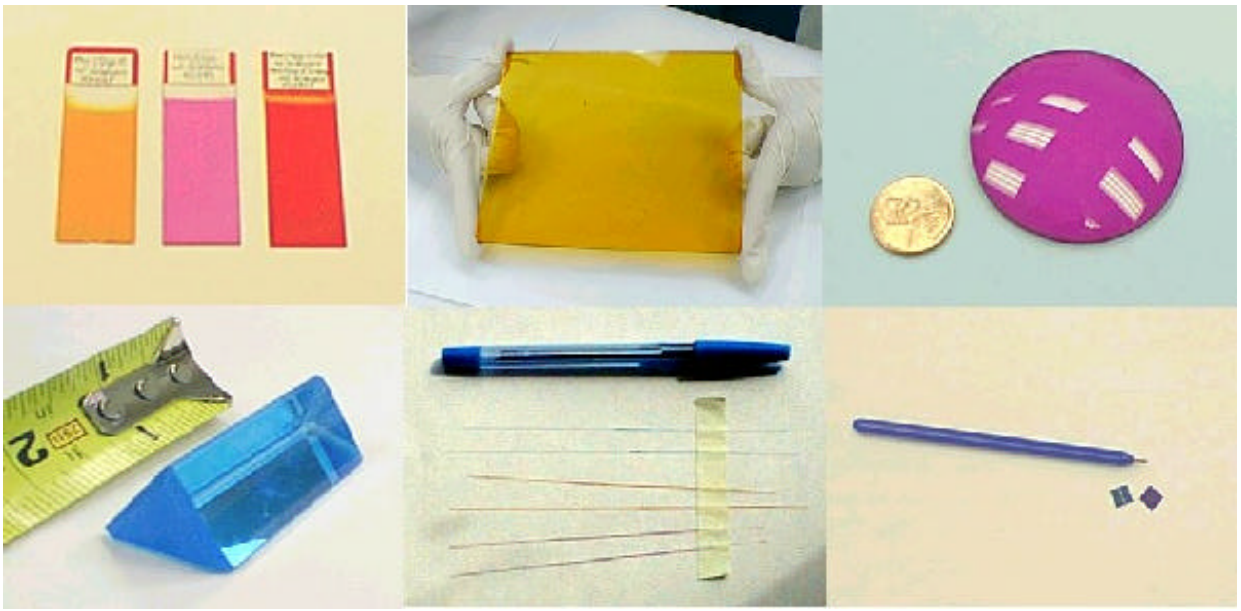

Figure 2-1. ESA films on various substrates.

The above pictures show that the ESA process can be applied equally well to substrates of almost any size or material and that the molecules self-assemble equally on all surfaces of the substrate. Uniform ESA films with over 2000 bilayers have been dipped in related ESA waveguide work.

The substrates require pretreatment before applying monolayers by the ESA process. The substrates of glass, quartz and single-crystal silicon types are cleaned with a "piranha solution," a 30:70 mixture of 30% hydrogen peroxide (H_2O_2) and concentrated sulfuric acid (H_2SO_4) at room temperature for 1 hour. Then they are extensively cleaned using ultrapure water, and dried in an oven at 50°C for several hours. After modification, the substrates are negatively charged. An ITO coated glass substrate is first cleaned using an ultrasonical system twice in ethanol. It is then immersed in a 1:1 mixture of ethanol:H_2SO_4 at room temperature for 1 hour and rinsed extensively in ultrapure water.

2.3 Multilayer dip processing procedures

Figure 2-2 shows the procedures of multilayer dip processing, which can be used equally well for the fabrication of coatings on structural materials or functional devices [2]. Before the dipping process, the substrate surface has been thoroughly cleaned and negatively charged through chemical processing. The charged substrate is dipped into an aqueous polycation solution, where polycation molecules are attracted to the anionic substrate surface and assemble themselves into a monolayer (a). The molecular order of such individual monolayers is nearly perfect, in much the same way that electrical charge on a free conducting surface distributes itself uniformly over the surface in order to minimize total system energy. Then the surface of the substrate is rinsed with ultrapure water to remove any loose particles, which may be held on the surface by weak van der Waals forces instead of ionic bonds. A polyanionic monolayer is deposited in the same manner (b), and subsequent layers are grown in bilayer pairs by alternately dipping the substrate in the polyanion and polycation solutions (c). Although Figure 2-2 suggests that each of the successive layers is a long polymer-like molecular chain, individual nanoparticles may be incorporated into any monolayer, allowing wide design opportunities for thin films with specific or multifunctional properties [3,4].

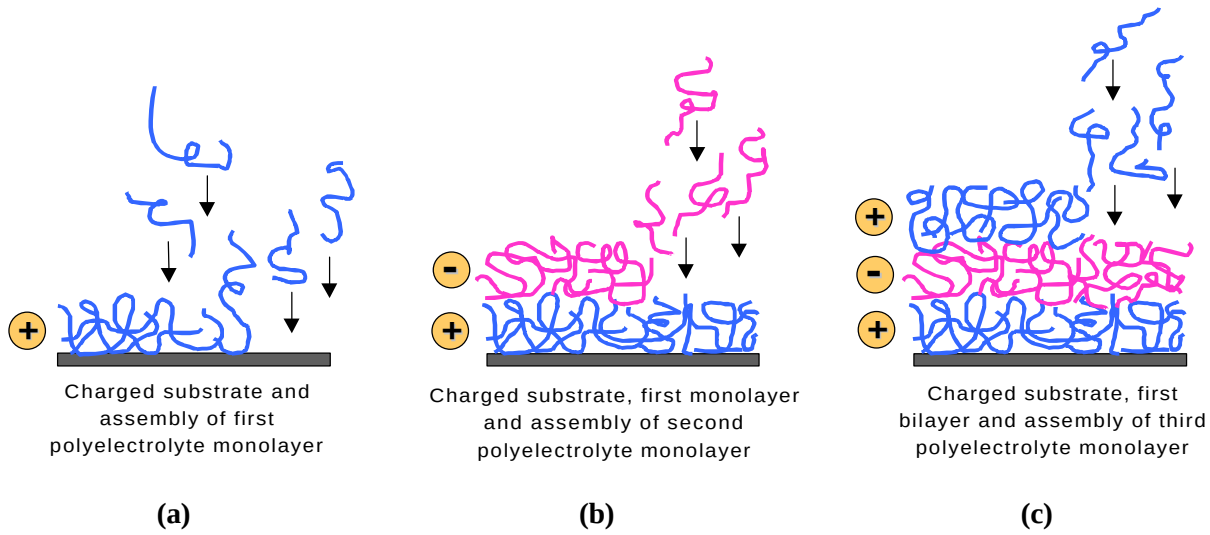

Figure 2-2. ESA procedures for buildup of multilayer assemblies by consecutive adsorption of anionic and cationic polyelectrolytes.

Before film synthesis, solutions of each film material are made by dissolving the polymers in acidic solutions and then adjusting the pH to a special value. Typically, the pH value of the solutions is 4.5 or 3.0.

An investigation on the effect of drying procedures and dipping time for each monolayer is discussed in the next two sections.

2.3.1 Drying procedures

In standard ESA processing, the film surface remains wet through all dipping steps. Experiments show that periodic drying to remove the water layer from the film surface will affect film characteristics.

Several pairs of Poly R-478/PDDA films were dipped on glass and single-crystal silicon substrates. For each pair, one specimen, labeled as “dried” in the graphs, was dried with nitrogen gas after the deposition of each monolayer; the second one was dried only for measurement

purposes, labeled as "undried". The differences of thickness and UV absorption between each pair are given in Figure 2-3 and 2-4 [2]. As shown in Figure 2-3, the thickness of the “dried” film is higher than “undried” one by 20%. Figure 2-4 shows a 15% increase of the optical absorbance with the drying procedure. The larger thickness and optical density in the “dried” film than the “undried” film suggests that the “undried” film possesses greater interpenetration between the monolayers, since the optical absorbance peak at 522nm is contributed only by the Poly R-478 molecules, not the PDDA molecules.

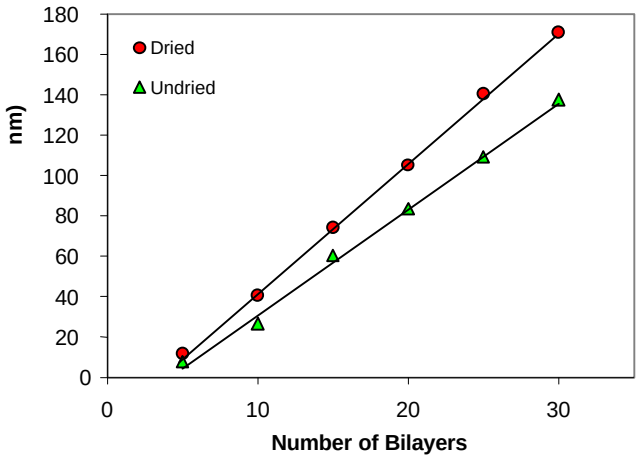

Figure 2-3. Thickness of Poly R-478/PDDA ESA films.

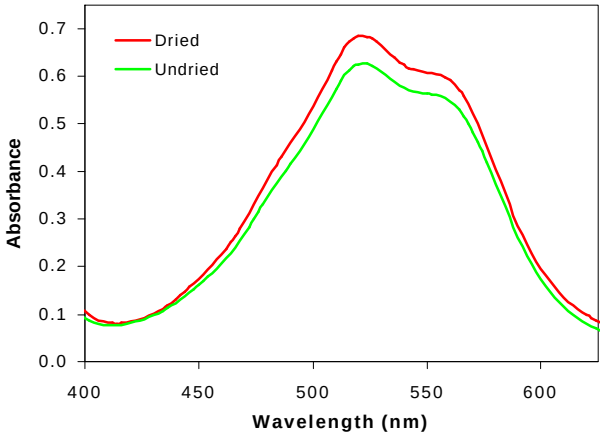

Figure 2-4. Absorption spectra of 50 bilayer Poly R-478/PDDA ESA films.

2.3.2 Dipping time

For each monolayer, the polyelectrolyte molecules require a certain amount of time to arrange themselves on the substrate and ionically bond to the substrate or film surface. The dipping time for each monolayer is an important factor to both research and commercial work, which is variable for different kinds of material and different concentration solutions.

Poly S-119/PDDA films, which were used for a number of the experiments in this work, were investigated with different dipping time for each monolayer. 1, 5, 10 and 20 minutes were used

to assemble 20 bilayer films on glass and silicon substrates, while concentration and pH values were identical for all samples. The thickness and UV/vis spectroscopy absorption for the samples are shown in Figure 2-5 and 2-6 [2].

Table 2-5 show the effect of dipping time on film thickness and optical absorption. All of the samples were fabricated by hand-dipping methods, and the total time required for bilayers includes both dipping process and rinsing process. A minimum of 1 minute is required for thorough rinsing by hand. Table 2-3 shows that although a 20-minute dipping time results in a 20% increase in thickness and optical density for each bilayer, the time required for each bilayer is increased by over 10 times.

Since the time is a critical value for research work as well as manufacturing, shorter dipping time process is highly attractive to achieve specific film properties. Typically, 1-minute dipping is adopted for the polymer dyes and PAH/PDDA or PSS systems, while for ZrO_2 nanoparticle/polymer composite systems, a 3-minute process is applied.

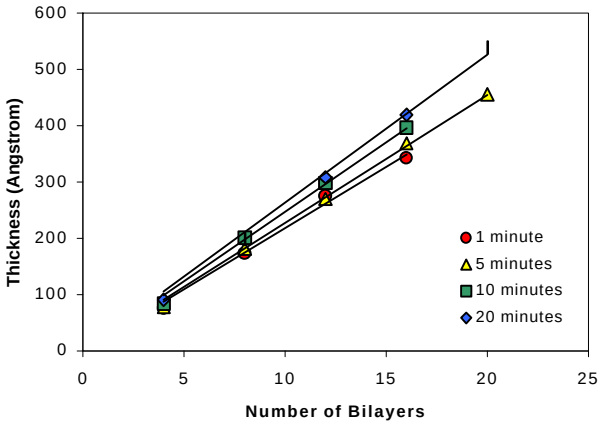

Figure 2-5 Thickness of PDDA/Poly S-119 ESA films with different dipping times.

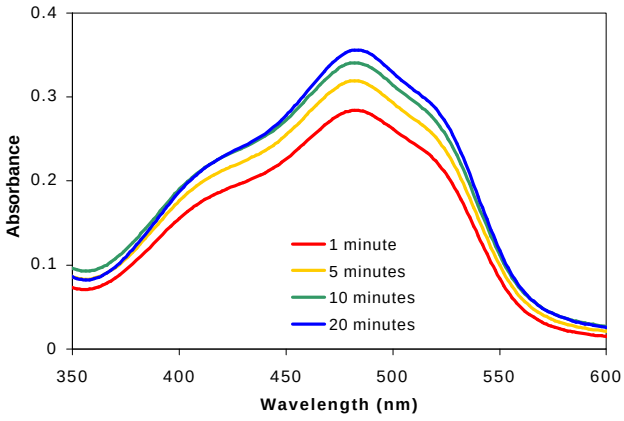

Figure 2-6 Absorption of 20 bilayers PDDA /Poly S-119 ESA with different dipping times.

Table 2-3. Effect of dipping time on film thickness and optical absorption.

DIPPING TIME (min)		1	5	10	20
Average thickness per bilayer (nm)		2.2	2.3	2.5	2.6
Average optical density per bilayer (a.u.)		0.0158	0.0180	0.0191	0.0193
Single bilayer	Minimum time required (min)	4	12	22	42
1 μm film	Number of bilayers required	458	440	404	380
	Minimum time required (hours)	31	88	148	266
1 a.u. optical density	Number of bilayers required	63	56	52	52
	Minimum time required (hours)	4	11	19	36

2.4 Characterization techniques

The ESA thin films were characterized and evaluated to determine structural, optical and secondary characteristics with emphasis on uniformity, film thickness, layer-by-layer linearity, surface morphology, thermal properties and optical characteristics, using the following materials analysis tools.

UV/vis spectroscopy: Multilayer ESA films were characterized using a Hitachi Model U-2010 UV/vis spectrophotometer to monitor film growth and uniformity, and determine the transmission and absorption spectral characteristics of films. Values reported are the average of measurements taken at three locations on each sample. The optical absorbance plots measured at several points during film growth gave a good indication of film quality and uniformity.

Ellipsometry: Multilayer films assembled on single-crystal Si substrates were measured using a Rudolph Auto-EL ellipsometer to determine the film thicknesses and refractive index. The instrument was calibrated using a standard silicon wafer with SiO_2 thickness 109.7 ± 0.3nm and index 1.462 ± 0.002. The reported values in this study were the average of

measurements taken at three locations, twice each. Thickness was a critical parameter in both the linear and nonlinear optical experiments.

Atomic force microscopy (AFM): A Digital Instruments NanoScope AFM was used in TappingMode™ to image the surface morphology of films with atomic resolution, utilizing topology and phase imaging in combination. Surface roughness analyses allowed the comparison and evaluation of different dipping techniques.

Contact angle: To determine the wettability and quality of monolayer and multilayer films, contact angle measurements were made using a Rame-Hart NRL Contact Angle Goniometer Model 100-00. The wettability of a film is dependent on the structure of the outermost few angstroms and thus can be used to verify the requisite reversal of surface charge with the addition of each monolayer in an ESA film. The measurements were taken at room temperature; the temperature was not controlled and so varied from 20-25°C. The drop volume was 4 μL and was placed on the film surface using a microliter syringe. The measurements were taken within 1 minute of drop application. The tangent to the drop was estimated visually. Each reported value was the average of 6 measurements taken on both sides of three drops.

2.5 Summary

This chapter investigated methods and properties of the ESA process itself. Each of the dip processing and film characterization methods was described in detail. ESA coating is demonstrated for various substrate sizes, shapes, and materials. The variables during processing procedures that can control the resulting film characteristics are investigated. The techniques for the thin film characterization are presented.

2.6 References

1. Y. Liu, *Characterization and Patterned Polymer Films from a Novel Self-Assembly Process*, Ph.D. dissertation, Chemistry Department, Virginia Polytechnic Institute & State University, May 1996.
2. K. Cooper, "Electrostatic Self-Assembly of Linear and Nonlinear Optical Thin Films", Ph.D. dissertation, Electrical Engineering Department, Virginia Polytechnic Institute & State University, Blacksburg, Virginia, May 1996.
3. G. Decher, Y. Lvov, J. Schmitt, "Proof of multilayer structural organization in self-assembled polycation-polyanion molecular films," *Thin Solid Films* 244, 772-7 (1994).
4. Y. Lvov, G. Decher and H. M. Hwald, "Assembly, Structural Characterization, and Thermal Behavior of Layer-by-Layer Deposited Ultrathin Films of Poly(vinyl sulfate) and Poly (allylamine)," Langmuir 9, 481 (1993).

Chapter 3 *TFCalc Simulation Software*

In the design of a thin-film multilayer, it is necessary to find a layer structure which will give a performance specified in advance. This process is much more difficult than straightforward calculation of the properties of a given multilayer. There is no analytical solution to the general problem [1-4]. The conventional method of design is to arrive at a possible structure for a filter, using several popular techniques, as follows:

- *The vector method*: This is a valuable method, especially in designing antireflection coatings. The length of the vector is the amplitude reflection coefficient at each interface and the direction of the vector indicates the phase shift. This method works under two assumptions – no absorption in the layers and only considering one reflection of the incident light at each interface. Thus the errors of this method may be high, especially where high overall reflectance from the multilayer exists, but they are small in most types of antireflection coatings.
- *Smith's method*: This technique is also known as the method of effective interfaces. It consists of choosing any layer in the multilayer and then considering multiple reflections within it, and this method can be extended to deal with absorbing layers beyond dielectric multilayers. Smith's method provides an insight into the properties of a particular type of filter, but it is certainly not the easiest way to determine the performance of a given multilayer.
- *The Smith Chart*: This chart presents circles of constant amplitude reflection coefficient and circles of constant real part and constant imaginary part of the reduced optical admittance. The Smith chart can simplify calculation.

Even given several useful techniques, the thin-film filter design is still difficult and tedious to carry out by hand. Therefore the modern design is completed with computer aided analysis. Provided a starting design, adjustments to the proposed design may be made, then recomputed, until a satisfactory solution is found. The successful application of refinement techniques depends largely on a starting solution; methods of completely automatic synthesis of designs without any starting point are seldom used. Because a number of parameters can potentially be involved, the possibilities without a starting design are virtually infinite.

Automatic design synthesis is undoubtedly increasing in application. TFCalc, Thin Film Design Software for Windows by Software Spectra, Inc., is such a kind of automatic thin-film optical filter design software kit. This chapter discusses TFCalc and is organized as follows. A brief introduction of TFCalc is given in section 3.1. Section 3.2 addresses the two primary functional properties of TFCalc - design optimization and sensitivity analysis.

3.1 Introduction to TFCalc

TFCalc is a commercial thin film design software for Windows, which is helpful for the evaluation of predesigned multilayer patterns and for the automatic design to meet specific performance requirements. The following diagram shows how to use the TFCalc program to design a thin film coating [5].

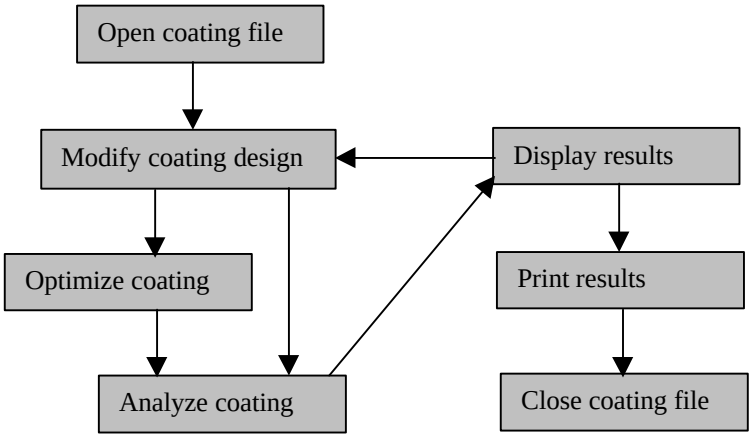

Figure 3-1. The flow diagram for thin film design by TFCalc.

Figure 3-2 illustrates the interface of TFCalc. Only the main menu and parts of the windows – Edit Environment, Front Layer, Plot and Table – are shown here.

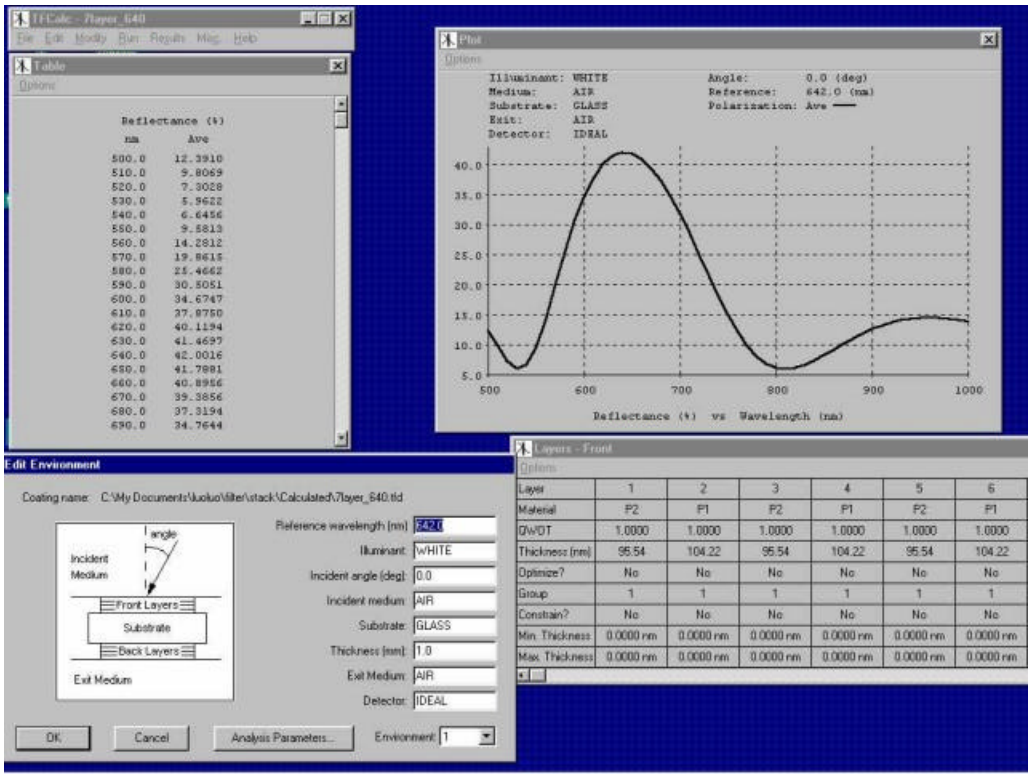

Figure 3-2. The interface of TFCalc.

Figure 3-3 shows the physical system modeled by TFCalc. The illuminant, stored in the Illuminant database, is given as a table of spectral intensity versus wavelength. The incident angle may vary from 0 to 89.999 degrees. The substrate and the incident and exit media are selected from the Substrate database. Both the substrate and the exit medium may be absorbing materials. The materials that compose the front and back layers are selected from the Materials database (or from a name in the Variable Materials window). Currently, there is a limit of 5000 layers. The optical properties of substrates and materials are stored as tables or dispersion formulas of complex refractive index (n-ik) versus wavelength.

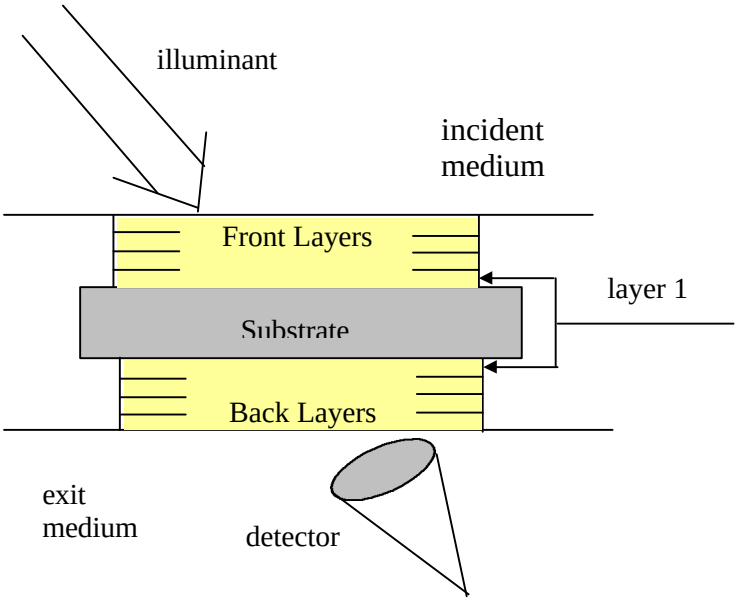

Figure 3-3. Schematic diagram of the physical system model by TFCalc.

The TFCalc program enables you to analyze and design multilayer thin film coatings. Some of its features are as follows [5].

- Reflectance, transmittance, absorptance, optical density, loss, color, luminance, phase shift on reflection or transmission, and electric field intensity may be computed and plotted.
- The sensitivity of the coating to manufacturing errors may be analyzed. Optimization can be used to minimize the sensitivity. Layer sensitivity can be computed and displayed.
- The coating materials, the substrate, and the exit medium may be dispersive and absorbing; the incident medium may be dispersive. Dispersion formulas can be used to give the index of materials and substrates.
- The refractive index (n and k) of a substrate or layer can be determined from measured data. The equivalent index may be calculated. Also a layer may be replaced by an equivalent (HLH)^p or (LHL)^p stack that matches the layer's index, where H and L are two different materials and p is the number of HLH or LHL stack.
- The illuminant and detector function may be specified. The reflectance or transmittance of a thin film may be stored as an illuminant, so that the output of one filter can be made the input of another. Also, blackbody illuminants may be created.

- The substrate may have a finite thickness; reflectance and transmittance calculations take into account the back surface of the substrate and any attenuation within the substrate.
- A coating may have up to 5000 layers, composed of up to 150 different materials. Stacks may be entered using a formula, such as H(LH)^5. Layers may be arranged in groups, and the groups may be optimized.
- Data for an unlimited number of materials, substrates, illuminants, and detectors may be entered.
- A choice of three local optimization methods are available: Gradient, Variable Metric, or Simplex. Global search may be used to locate the best design, rather than just the local minimum.
- The results of six thin film calculations may be compared by plotting them on the same graph. Different types of plots may be overlaid: e.g., reflectance and transmittance. The minimum, maximum, and average values of a parameter can be computed for a range of wavelengths. Results may be saved to text files for processing by other software.
- Multiple environments can be used to develop, for example, coatings for multiple substrates.
- A coating can be analyzed for a cone of angles (as in a convergent beam of light).
- Optical monitoring curves can be computed and plotted.

3.2 Main properties of TFCalc

Possessing many useful features introduced in the previous section, TFCalc is a good tool to help the designer analyze and design optical thin films. This section discusses two powerful features frequently used in this thesis work – design optimization and sensitivity calculation.

3.2.1 Design optimization

A choice of three local optimization methods are available: Gradient, Variable Metric, or Simplex. Layers on both sides of the substrate may be optimized simultaneously. Up to 1000 optimization targets may be specified.

The Optimize Design command tells the program to vary the thickness of the layers or the group factor of groups (and the index of variable materials) so that the following merit function is minimized:

$$F = \left(\frac{1}{m} \sum_{i=1}^{m} \left| I_i D_i \left(\frac{T_i - C_i}{N_i Tol_i} \right)^k \right| \right)^{1/k} \qquad \textbf{(3.1)}$$

where m is the number of targets, k is the power of the method, I is the intensity of the illuminant, D is the efficiency of the detector, T is the desired target value, C is the computed value (of reflectance, transmittance, etc.), Tol is the tolerance for a target, and N is the normalization factor for the target. The purpose of N is to convert the units to a compatible scale. In most cases, I = D = Tol = 1.0. The quantity (T - C) / N is called the "deviation from target". The number k, termed the power of the method, can have a significant effect on the optimization results. The program allows the following values for k: 1, 2, 4, 8, 16, and higher value. As the value of k is increased, the larger deviations will be emphasized, forcing the optimization methods to equalize the deviations of the targets.

Global search may be used to locate the best design, rather than just the local minimum. Needle optimization can add layers to a design automatically, which is very useful if the design's requirements are unusual. The tunneling method can be used to automatically generate a sequence of optimal designs.

Table 3-1 and 3-2 gives six different designs with or without optimization. The corresponding reflectance spectra are illustrated in Figures 3-4 and 3-5. In A.1, all three layers are a quarter wavelength thick at the reference wavelength of 550nm, and there is not any optimization of thickness and refractive index. Only the index of the first layer is optimized in A.2, while for A.3, the thickness of all layers plus the index of the first layer is optimized. The continuous target set for A.2 and A.3 is that the reflectance within the range of 400nm to 800nm is zero. For the other three designs, 41 discrete targets are used with uniform steps of 10nm. The gradient of simplex optimization method is used during the design. The graphs show the strong ability, provided by TFCalc, of reaching the desired design to achieve the specific performance by adjusting the optimization target or method.

Table 3-1. Three design examples with or without optimization.

		Material	N	Index optimize?	QWOT	Thickness (nm)	Thickness optimize?
A.1	Layer 1	M*	1.66	No	1	82.83	No
	Layer 2	H*	1.68	No	1	81.85	No
	Layer 3	L*	1.54	No	1	89.29	No
A.2	Layer 1	M	1.6343	Yes	1	84.14	No
	Layer 2	H	1.68	No	1	81.85	No
	Layer 3	L	1.54	No	1	89.29	No
A.3	Layer 1	M	1.6246	Yes	0.9272	78.47	Yes
	Layer 2	H	1.68	No	1.4260	116.71	Yes
	Layer 3	L	1.54	No	1.0572	94.39	Yes

Table 3-2. Three design examples with optimization.

		Material	N	Index optimize?	QWOT	Thickness (nm)	Thickness optimize?
B.1	Layer 1	M*	1.6005	Yes	0.8945	76.85	Yes
	Layer 2	H*	1.68	No	1.0071	82.43	Yes
	Layer 3	L*	1.54	No	0.9884	88.25	Yes
B.2	Layer 1	M	1.584	Yes	1.0338	89.74	Yes
	Layer 2	H	1.68	No	0.9272	75.89	Yes
	Layer 3	L	1.54	No	0.9489	84.72	Yes
B.3	Layer 1	M	1.598	Yes	1	86.04	Yes
	Layer 2	H	1.68	No	1	81.85	Yes
	Layer 3	L	1.54	No	1	89.29	Yes

H: PDDA/Poly S-119; L: PDDA/PSS; M: Combination of H and L.

QWOT: quarter-wave optical thickness

Reference wavelength: 550.0nm.

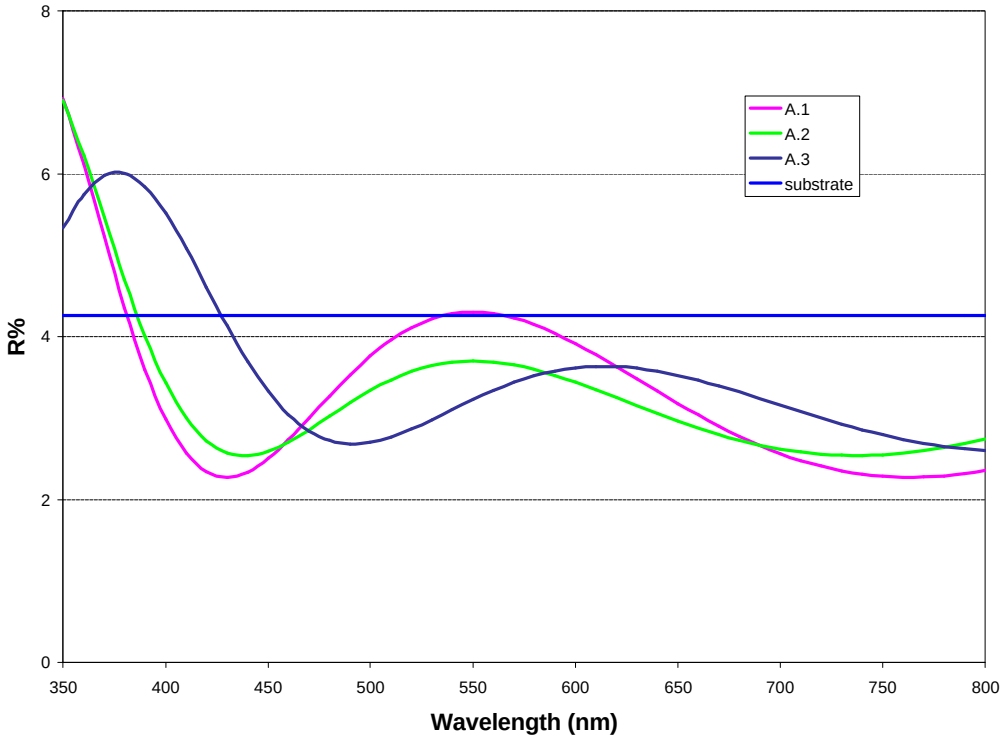

Figure 3-4. Simulated reflectance spectra for the different designs with or without optimization.

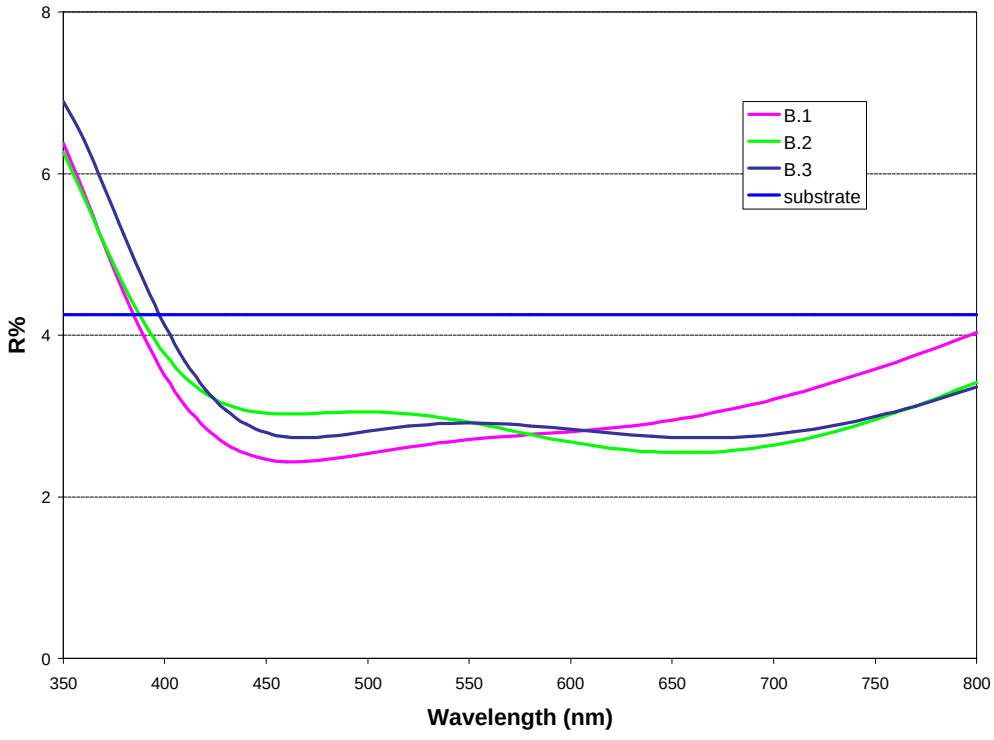

Figure 3-5. Simulated reflectance spectra for the different designs with optimization.

3.2.2 Sensitivity analysis

Compute Sensitivity commands the program to determine how sensitive the coating design is to small manufacturing errors (also called tolerancing). The expected error of thickness or refractive index and the number of trials can be set by the designer. The sensitivity computation selects thicknesses or indices that are uniformly or normally distributed within the error range. The program will vary the thicknesses or indices of layers randomly, analyze the coating design by the Monte Carlo method, and record the results.

Figures 3-6 and 3-7 illustrate film sensitivity to a thickness error of ±5nm and relative index error ±0.3% for pattern B.3. The heavy center line represents the original coating design; the two outer-most lines above it and below it represent the minimum and maximum (that is, the worst-case) variation as the layer thicknesses or indices are varied randomly. If the "quartile" sensitivity analysis, instead of "worst-case", is selected, then three additional curves are computed and displayed: the first, second, and third quartiles. The second quartile is the median performance (which is usually very close to the performance of the coating design). The first and third quartile curves are usually slightly below and above the median performance.

Layer sensitivity can also be calculated. This function lets the user determine which layers are most sensitive to manufacturing errors. It is generally used only after a design has been completely optimized. A bar chart is produced, as shown in Figure 3-8. There are two cases to consider for the chart: (1) When computing the layer sensitivity of a completely optimized design, the first-order sensitivity is very close to zero. In this case, the second-order sensitivity indicates the steepness of the valley in which this design lies. If a layer has a large second-order sensitivity, it means that a small change in that layer's thickness will lead to a large increase in the value of the merit function (3.1). (2) When this computation is applied to a non-optimized design, then the second-order sensitivity is undefined. In this case, the first-order sensitivity shows how the merit function increases or decreases as thickness increases. Figure 3-8 is the layer sensitivity for B.3, which shows that the first-order sensitivity is almost zero, and the top layer is most sensitive to manufacturing errors. Minimized sensitivity can be selected in the optimization parameters.

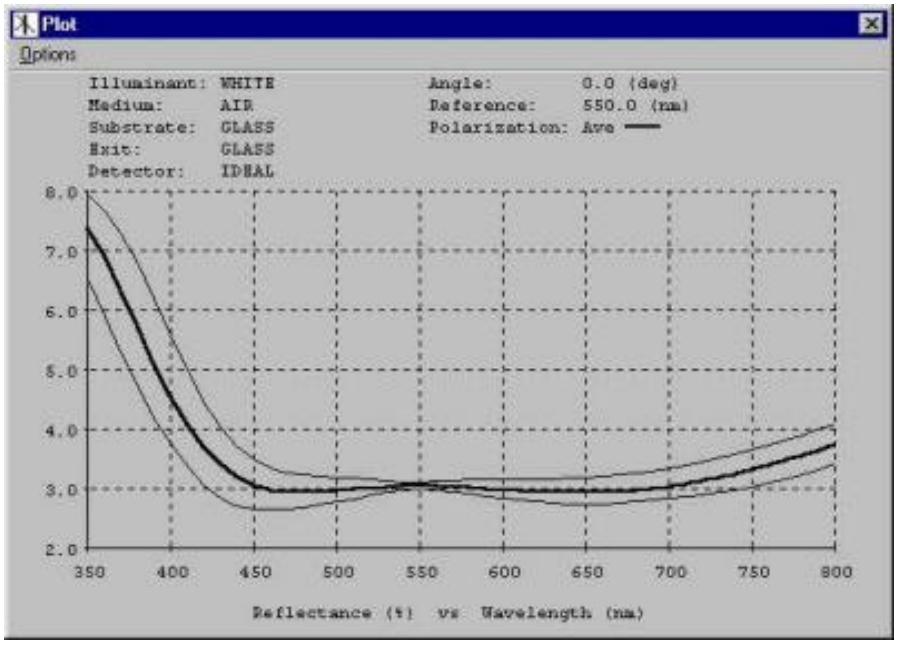

Figure 3-6. Film sensitivity to the thickness error of ±5nm for B.3.

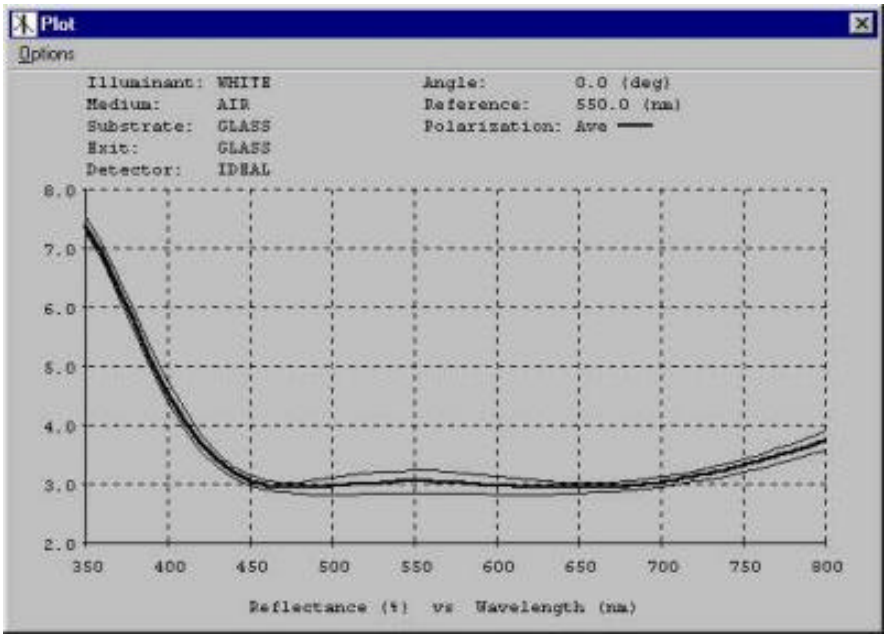

Figure 3-7. Film sensitivity to the relative index of ±0.3% for B.3.

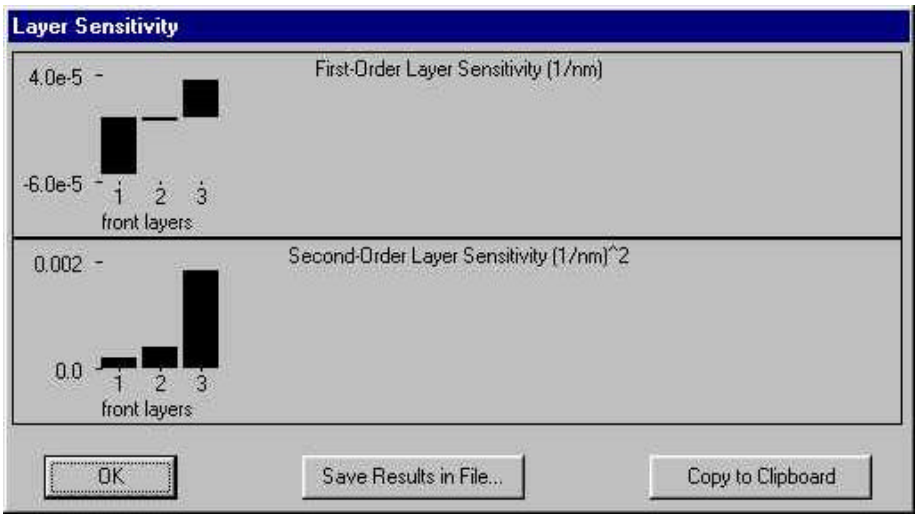

Figure 3-8. Layer sensitivity for B.3.

3.3 Summary

TFCalc, a powerful thin film design software, is introduced in this chapter, and the two primary functional features – design optimization and sensitivity analysis- are addressed in detail. This software is used in the design and evaluation of the optical thin film filter discussed in the next chapter.

3.4 Reference

2. H.A. Macleod, *Thin-Film Optical Filters*, McGraw-Hill, New York (1989).
3. A. Thelen, *Design of Optical Interference Coatings*, McGraw-Hill, New York (1989).
4. R.R. Willey, *Practical Design and Production of Optical Thin Films*, M. Dekker, NY (1996).
5. C.K. Madsen, J.H. Zhao, *Optical Filter Design and Analysis: a Signal Processing Approach*, John Wiley, NY (1999).
6. TFCalc, Thin Film Design Software for Windows manus, Software Spectra, Inc., (1995).

Chapter4 *Linear Optical Filters Formed by ESA*

Optical interference filters have been studied since the early 1800s when the principle of the interference of light was first explained by Thomas Young. Fraunhofer fabricated the first recognized antireflection coatings in 1817. The theoretical basis for the analysis of such optical thin films was provided by James Clerk Maxwell's system of equations, first published in 1873. Optical thin films are extensively applied to optical systems, including cameras, binoculars, telescopes, microscopes, spectacle lenses, display windows, picture frames and laser systems, as well as applications which require increased light capture such as solar cells, detectors and magneto-optical devices [1,2].

Optical filters or coatings can be defined as thickness-dependent refractive index systems which modify the properties of a surface to produce the desired optical characteristics. They can work over a broad range of wavelengths, or a very narrow band. Figure 4-1 illustrates a single thin-film optical filter. To qualitatively understand the performance of thin-film optical devices, several simple concepts are necessary to present [3].

1. The light amplitude reflected at a boundary between two media, when normally incident, is given by (1-ë)/(1+ ë), where ë is the ratio of refractive indices of the materials on either side of that boundary.
2. There is a π phase shift when the reflection takes place within the lower index material and zero if the medium has a higher index than the one adjacent to it.
3. The incident light will be reflected from both the top and bottom surfaces of a thin film, then the beams will recombine either constructively or destructively. In the case of constructive recombination, the result beam is the sum of the amplitudes if the relative phase shift is either

zero or a multiple of 360°. If the relative phase shift is an odd multiple of 180°, the combination is the difference of the two beams. Other cases where the phase shift is different will be intermediate between these two possibilities.

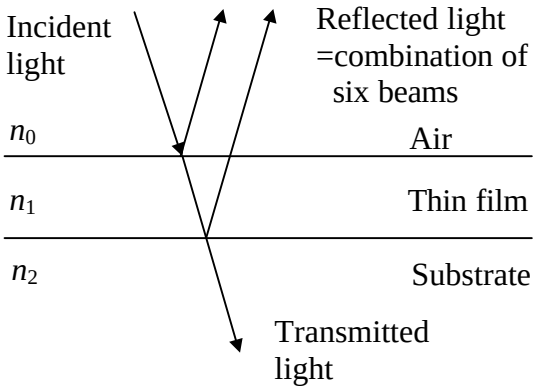

Figure 4-1. A single thin film.

Practical application of optical thin film filters also requires mechanical properties such as hardness and abrasion resistance, as well as chemical and environmental durability. Vacuum evaporation and sputtering are two main commercial approaches to fabricate the optical thin film. These methods require big equipment, including vacuum chambers, power supplies, requisite pumps and pressure gauges. Coating uniformity depends on a number of geometric considerations and physical conditions. In these processes, substrate materials and size are limited, since substrates are usually heated to increase the molecule's energy, allowing the molecules to arrange themselves to a low energy lattice site before being incorporated into the film [4-8]. Another obstacle is the potential mismatch in thermal expansion coefficients between the substrate and coating.

The ESA process offers significant advantages over conventional thin film fabrication methods. Much like the behavior of electrons on conductive surfaces, the polyelectrolyte molecules arrange themselves uniformly across the charged surface. The molecular-level uniformity achieved in each monolayer permits precise control of thickness, refractive index and other properties. Extremely homogeneous mixtures of inorganic nanoparticles, polymers, as well as organic molecules can be incorporated into each monolayer, allowing nanoscale

control of film optical, electronic, magnetic, mechanical and multifunctional properties. The ionic bonding of molecules produces stable thin films on substrate surfaces of arbitrary shape and size. Moreover, equipment costs for ESA process are much lower than traditional methods, for it does not require large equipment. Fabrication by ESA only consists of repeatedly dipping the substrate into aqueous solution baths at room temperature.

The feasibility of the ESA process for the fabrication of linear optical interference filters with enhanced properties is demonstrated in this chapter. The chapter is organized as follows. Section 3.1 shows how ESA process precisely controls the thickness and refractive index of multilayer thin films. Design and synthesis of dielectric stack filters and antireflection coatings with improved performance are discussed in Section 3.2 and 3.3 respectively. A brief summary about the linear optical filters by ESA is provided in Section 3.4.

4.1 Control of refractive index profile by ESA

This section demonstrates the feasibility of control of the refractive index of thin films by combining multiple materials in ESA film. Single anion/single cation ESA films with a range of refractive indices are investigated first, followed by the study of combined multiple anions and/or cations in a single film to implement graded index structures by varying the material components through the film thickness.

First, single anion/single cation, or ABAB configuration ESA films with a range of refractive indices are assembled. Table 4-1 shows the refractive index and thickness parameters for 50 bilayers of PDDA/PSS, PDDA/Poly S-119 and PDDA/Direct Red75. Figures 4-2 and 4-3 illustrate the linear growth of both optical absorption and film thickness with the number of layers, which indicates that each bilayer contributes equally to the whole film, both in optical density and thickness [6]. Homogeneous fabrication for each bilayer is demonstrated.

Table 4-1. Refractive index and thickness for 50-bilayer ESA films.

	Anion	Cation	n			Average Bilayer Thickness (nm)
			632.8 nm	546.1 nm	405.0 nm	
1	PSS	PDDA	1.539	1.538	1.559	2.3
2	Direct Red 75	PDDA	1.767	1.629	1.662	1.2
3	Poly S-119 (Sigma)	PDDA	1.682	1.799	1.535	2.8

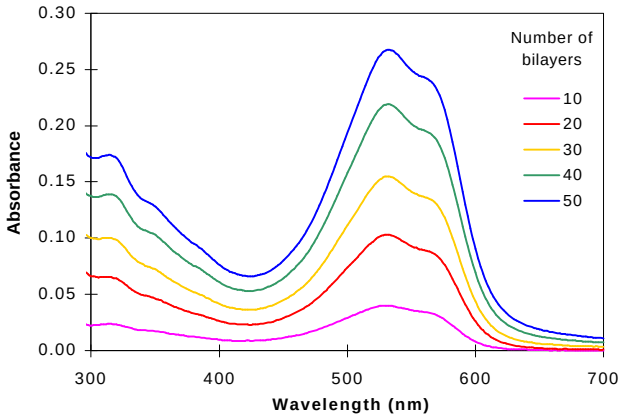

Figure 4-2. UV/vis absorbance of Direct Red 75 / PDDA ESA thin films.

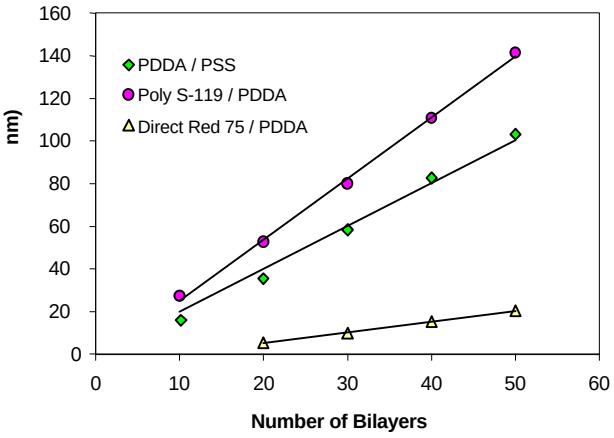

Figure 4-3. Film thickness with increasing numbers of bilayers.

A small thickness dependence was found in the refractive index for the first few hundred Ångstroms of film growth, followed by saturation after approximately 40-50 bilayers. It is believed this is due to an equipment limitation at film thicknesses less than 500 Å rather than a true material characteristic. Figure 4-4 illustrates the wavelength and thickness dependence of the film indices. It is clear that PDDA/PSS films exhibit the most uniform dispersion spectrum.

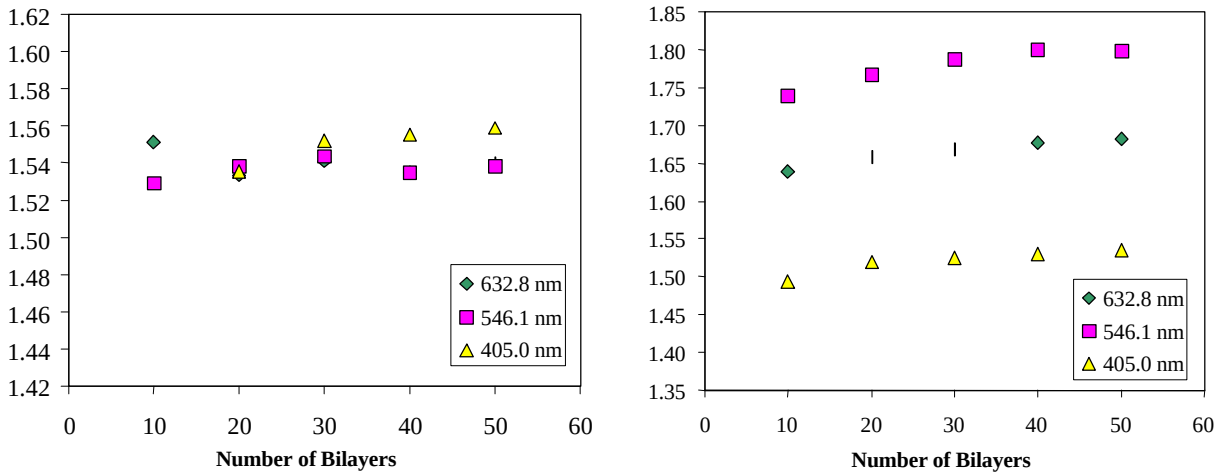

Figure 4-4. Wavelength and thickness dependent refractive index (Left: PDDA / PSS; Right: Poly S-119 / PDDA).

In order to achieve a graded index structure, multiple anions and/or cations are combined in a single film by varying the material proportions. Figure 4-5 illustrates the concept of building up multilayers composed of predetermined patterns of Direct Red 75/PDDA (X) and PSS /PDDA (Y), specifically a mixture of 33% X and 67% Y (XYY configuration) [6]. The UV/vis absorbance spectra of 50-bilayer multilayer films with increasing X percentage from 0% to 100% are shown in Figure 4-6. It is clear that absorbance increases linearly for each film, indicating that each multilayer is an identical, reproducible unit, and therefore a suitable ESA building block. Theoretical and measured refractive indices at the wavelength of 632.8nm for varying X percentage multilayer films are shown in Figure 4-7, which demonstrates that it is possible to grade the index n(x) by varying the X percentage through the thickness of a film. The multilayer films are a nearly linear combination of the individual X and Y films, and the refractive index of ESA thin films can be controlled by appropriately designing multilayer structures. This is the basis of thin-film refractive index control using the ESA process.

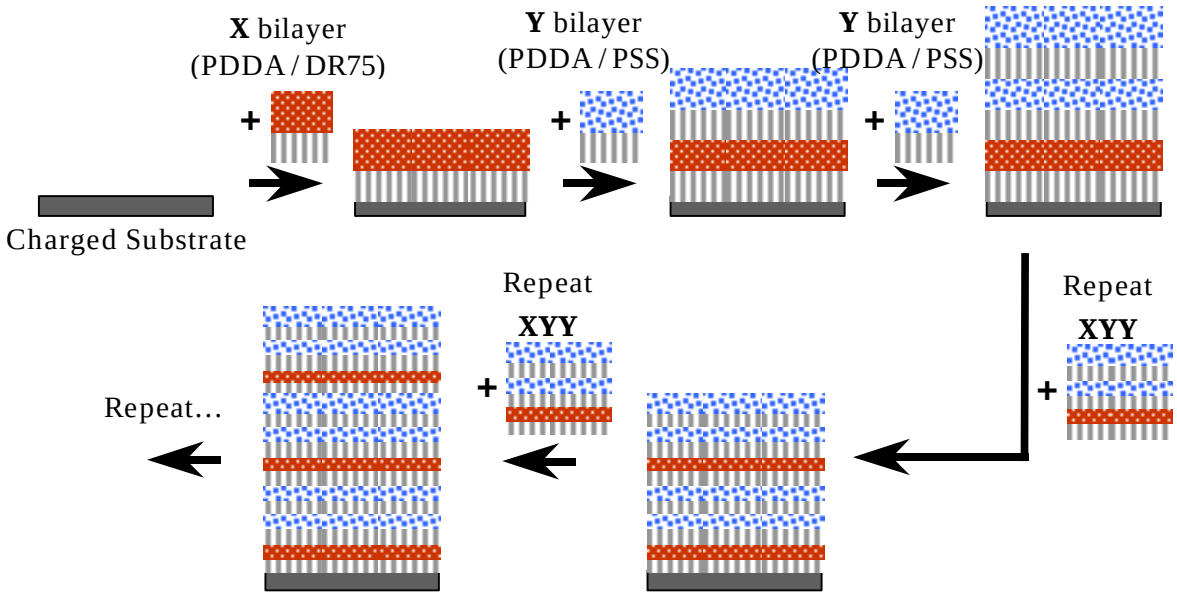

Figure 4-5. Process of the self-assembly of 33:67 mixture (XYY multilayer) ESA thin films.

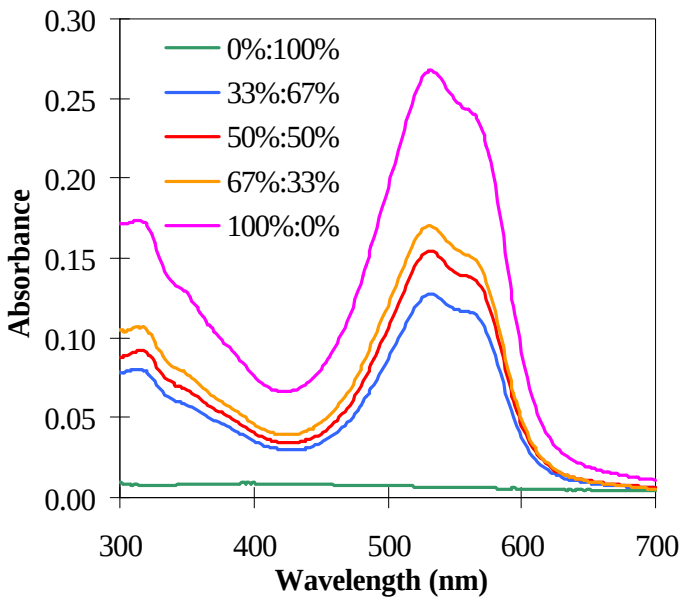

Figure 4-6. UV/vis spectra for increasing X:Y [(PDDA /Direct Red 75):(PDDA/PSS)] ratios in 50-bilayer films.

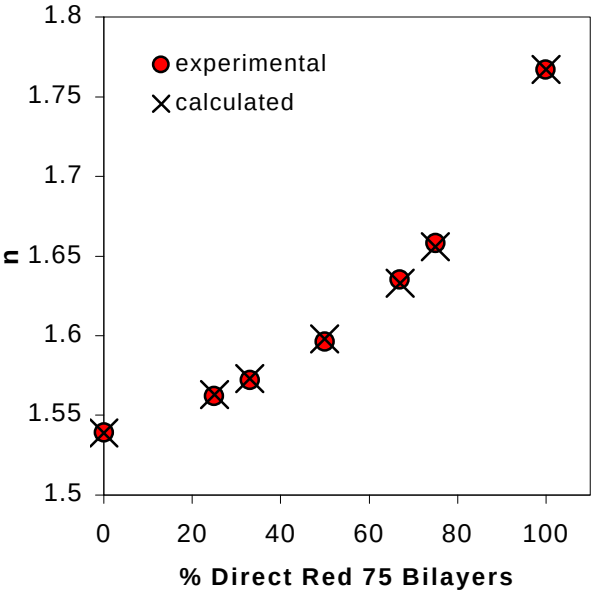

Figure 4-7. Bulk refractive index vs. percentage of PDDA /Direct Red 75.

4.2 Dielectric stack filters

A dielectric stack filter is a basic type of thin-film structure, which is a stack of alternate high- and low-index films each one quarter wavelength thick, as shown in Figure 4-8. Light reflected in the layers of high-index will not suffer any phase shift, while those reflected within the low-index layers will suffer a 180° shift. It is easy to show that the beams reflected from all the interfaces are of equal phase when they reach the front surface, so they will recombine constructively. This implies that the effective reflectance of the stack can be achieved as high as desired, just by increasing the number of the layers. This is a basic form of high-reflectance coating.

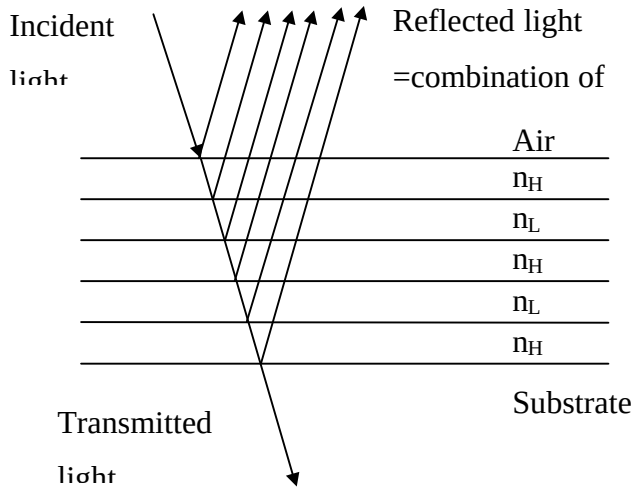

Figure 4-8. Quarter-wave stack.

It is found that the reflectance of the dielectric stack filter remains high over a limited range of wavelengths, depending on the ratio of high and low refractive indices. Outside that range, the reflectance decreases quickly to a low value. Due to this property, the quarter-wave stack is used as a basis for many types of thin-film filters, such as longwave-pass filters, shortwave-pass filters, Fabry-Perot (FP) filters [3]. FP filter consists of a spacer layer which is usually half a wavelength thick, bounded by two high-reflectance stacks, allowing extremely high transmission over a narrow band of wavelengths.

A stack of alternating high (H) and low (L) index layers, each of optical thickness λ/4, is considered. The first layer, next to the substrate and the outermost layer must be high-index. The maximum reflectance in air for such a stack is given by [3]

$$R_{\lambda/4} = \left(\frac{1-(n_H/n_L)^{2p}(n_H{}^2/n_S)}{1+(n_H/n_L)^{2p}(n_H{}^2/n_S)} \right)^2 \qquad \textbf{(4.1)}$$

where n_H, n_L and n_S are the indices of the high-, low-index layers and substrate respectively. There are a total of $(2p+1)$ of layers in the stack. The greater the number of layers the greater the reflectance.

Provided the materials are transparent and possess negligible absorption in the multilayer stack, and $(n_H/n_L)^{2p}(n_H{}^2/n_S) > 1$, then

$$\begin{aligned} R &\approx 1-4(n_L/n_H)^{2p}(n_S/n_H{}^2) \\ T &= 1-R \approx 4(n_L/n_H)^{2p}(n_S/n_H{}^2) \end{aligned} \qquad \textbf{(4.2)}$$

which shows that where reflection in high, the addition of two low- and high-index layers reduces the transmission by a factor of $(n_L/n_H)^2$.

The reflectance spectrum for a typical quarter-wave stack is shown in Figure 4-9 [3]. It is clear that the high-reflection zone is limited in extent. The reflectance spectrum falls sharply to a low, oscillatory value beyond the zone. The additional set of high- and low-index layers does not affect the width of the zone of high reflectance, but increases the magnitude of peak reflectance as well as the number of sideband oscillations. The width of the high-reflectance zone is given as

$$\Delta f = \frac{4}{\pi} \sin^{-1}\left(\frac{n_H/n_L - 1}{n_H/n_L + 1} \right) \qquad \textbf{(4.3)}$$

which shows that the zone width is only dependent on the ratio of refractive indices of the high and low index layers. The higher the ratio, the greater the width.

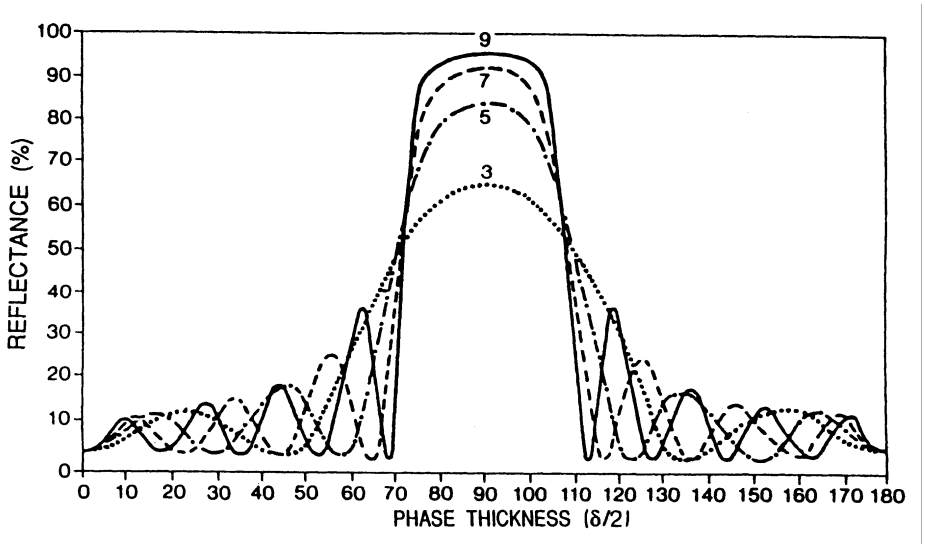

Figure 4-9. Theoretical reflectance spectra for multilayer stacks of alternating $l/4$ layers of n_H=2.3 and n_L=1.38 on glass (n_S=1.52) as a function of phase thickness ($2pnd/l$). The number of layers is indicated.

Based on the above theory and the refractive index data discussed before, a dielectric stack filter was designed after simulating using TRCalc software and was synthesized using ESA methods by hand. The high-index λ/4 material is the set of PDDA and Poly S-119 (Sigma), with n=1.68 at 633 nm, while the low-index one is the set of PDDA and PSS, with n=1.54 at 633 nm. Figure 4-10 shows the prototype of the dielectric stack filter and refractive index profile, and Table 4-2 presents the structure for each layer.

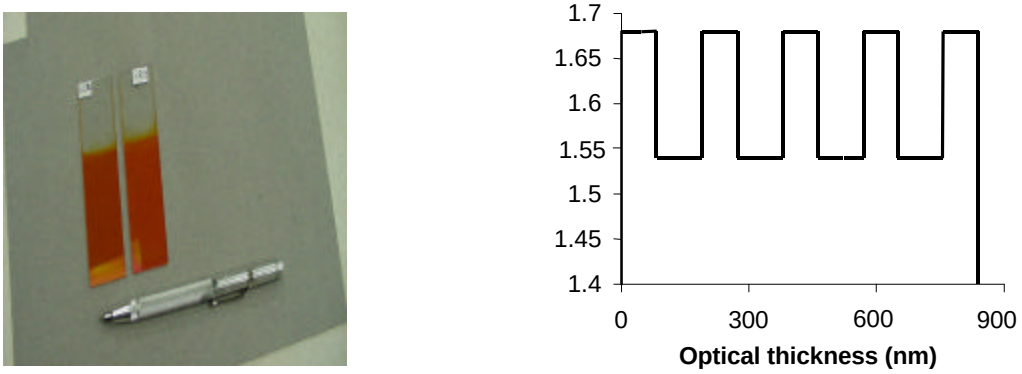

(a) **(b)**

Figure 4-10. (a) Dielectric stack filter
(b) Refractive index profile.

Table 4-2. Structure of dielectric stack filter.

(H: PDDA/Poly S-119; L: PDDA/PSS)

Reference wavelength: 642nm

	Layer 1	Layer 2	Layer 3	Layer 4	Layer 5	Layer 6	Layer 7
Material	H	L	H	L	H	L	H
n	1.68	1.54	1.68	1.54	1.68	1.54	1.68
QWOT	1	1	1	1	1	1	1
Thick (nm)	95.54	104.22	95.54	104.22	95.54	104.22	95.54
# of bilayers	34	45	34	45	34	45	34

The simulated reflectance spectrum and measured reflectance for the dielectric stack filter are shown in Figures 4-12 and 4-13, respectively. Both the magnitude of the reflectance peak and the number of sideband oscillations increase with an increasing number of λ/4 layers, which shows a significant agreement between the simulation and experimental result. Figure 4-11 illustrates the peak values for the simulation and experiment.

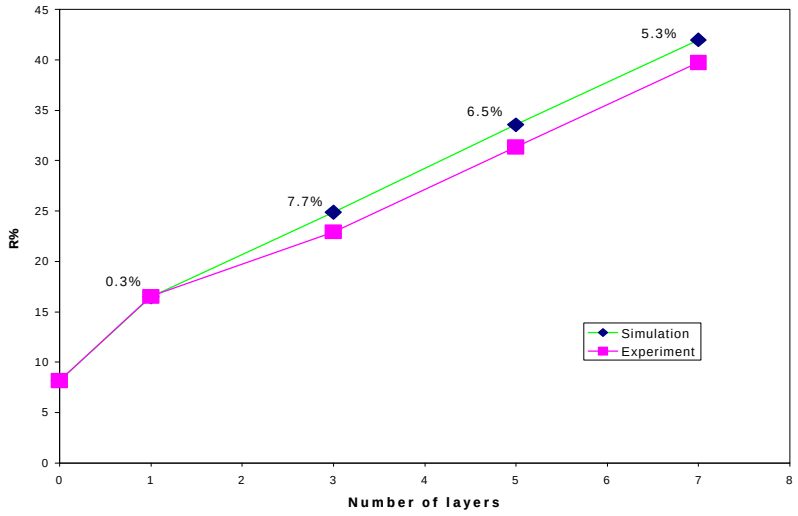

Figure 4-11. Reflectance peak value for dielectric stack filter. The difference between simulation and experiment is indicated for each layer.

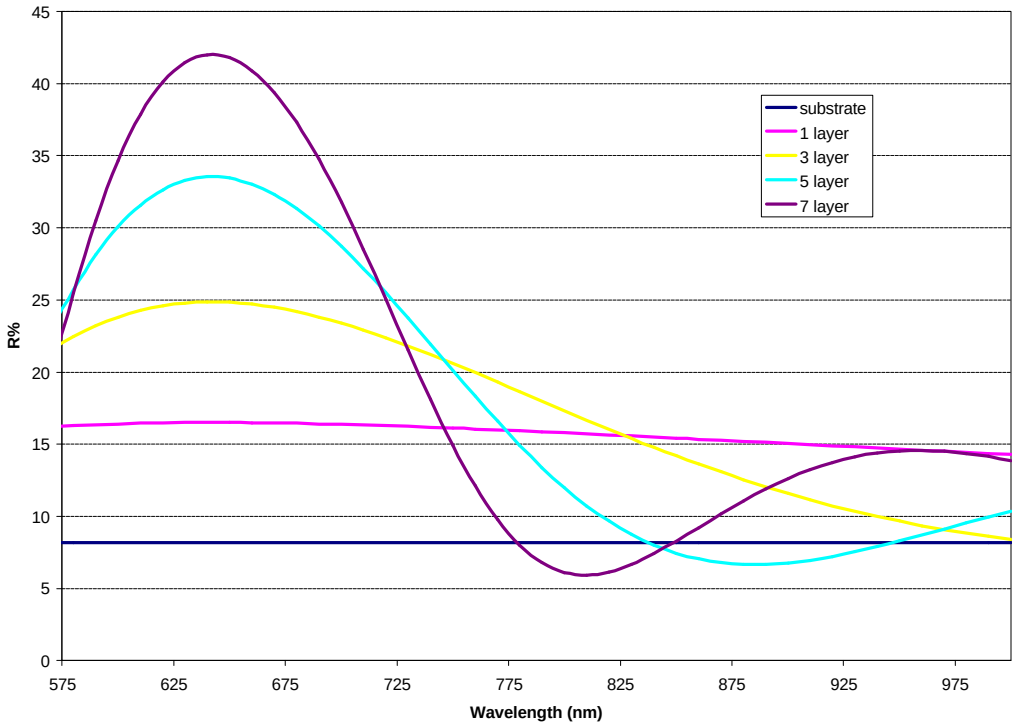

Figure 4-12. Dielectric stack filter simulated reflectance spectrum for increasing numbers of λ/4 layer.

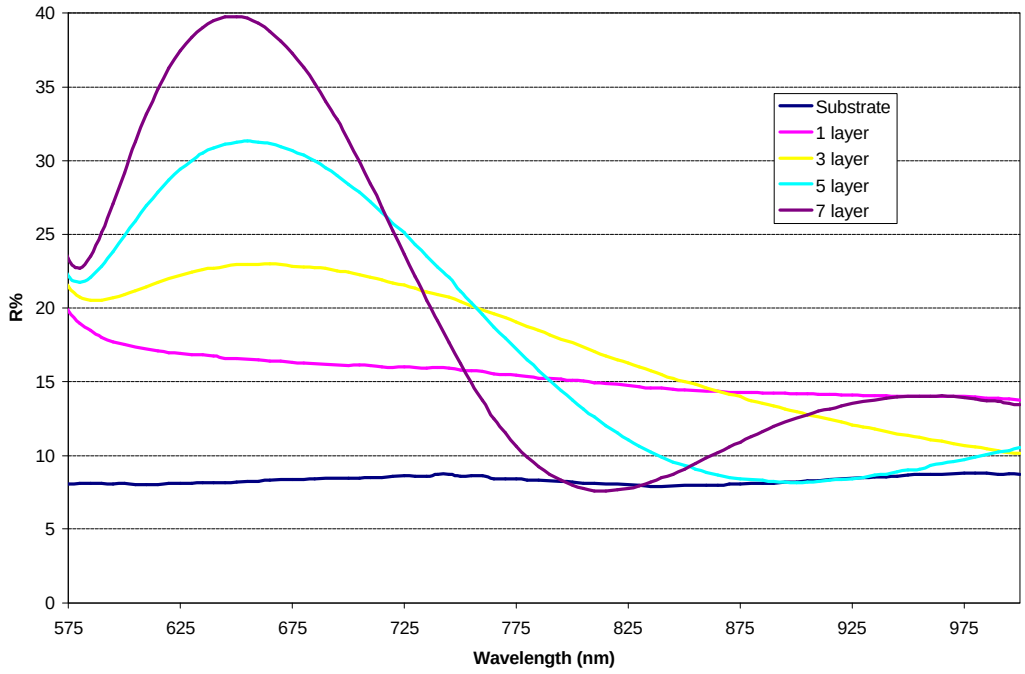

Figure 4-13. Dieletric stack filter experimental reflectance spectrum for increasing numbers of λ/4 layer.

These dielectric stack filters require each layer to be exactly λ/4 thick. The simulation assumes that the refractive index is exactly uniform for each layer. The following two figures illustrate the sensitivity to the absolute variable thickness ±5nm and relative variable index ±0.2%.

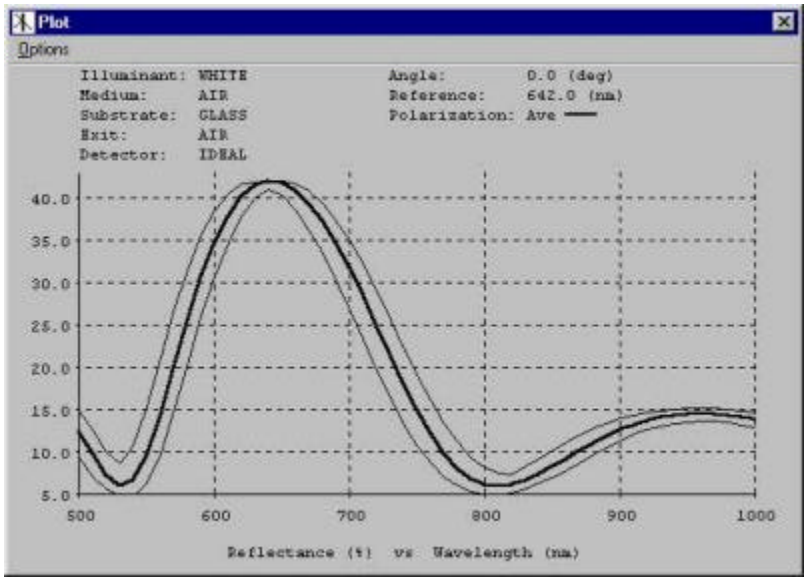

Figure 4-14. Calculated sensitivity to the absolute variable thickness ±5nm for 7 layer stack.

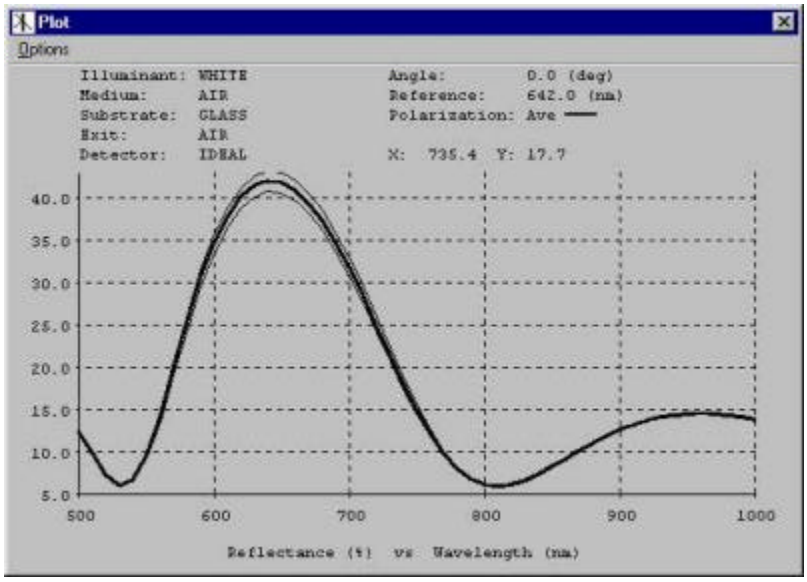

Figure 4-15. Calculated sensitivity to the relative variable index ±0.2% for 7 layer stack.

The total thickness of the simulated 7 layer stack is 694.8nm, while the measured thickness is about 690nm. The above sensitivity calculation shows that the experiment result significantly matches the bottom curve in Figure 4-14, which demonstrates the feasibility of precisely control the thickness and refractive index by ESA methods.

This work greatly enhanced the previous dielectric stack filter design and synthesis [6]. The reflectance magnitude for the corresponding layer increased by over 2 times, and a more consistent peak wavelength is obtained. One of the possible reasons is that the previous design mixed up the optical thickness with physical thickness. Each layer in the stack is equally a quarter-wave in thickness, which is optical thickness. The physical thickness for each layer should not be equal considering the different index.

Table 4-3. Peak reflectance comparison between previous and current design.

	1 layer	3 layer	5 layer	7 layer
Previous design (%)	3.5	7.0	12.0	17.0
Current design (%)	16.55	22.95	31.35	39.77

The spectral width of the high-reflectance zone is dependent on the ratio of refractive indices between the two layers, in this case, approximately 1.091.

4.3 Antireflection (AR) filters

Antireflection filters are another principal type of structure in thin-film optics. In some applications, AR coatings are simply required for the reduction of surface reflection, while in others, not only must surface reflection be reduced, but the transmittance must also be increased. AR coatings are widely used in optical components, such as telescopes, microscopes, binoculars, cameras, spectacles, as well as new applications that have emerged with the growth of other technologies, e.g. solar cells, laser systems and automobile glasses.

The operation of AR coatings depend on the more or less complete cancellation of the light reflected at all of the surfaces of the film. Considering the simple single layer filter in Figure 4-1, the intensities of the reflected light from the upper the lower surfaces of the film should be equal in order to complete cancellation of the reflection. This implies that the ratios of the refractive indices at each surface should be equal, i.e. $n_0/n_1 = n_1/n_2$, or $n_1 = (n_0 n_2)^{1/2}$. Meanwhile, the optical thickness of the film should be $\lambda/4$ to ensure that the total phase shift is 180° [3].

AR coatings can be a simple single layer with almost zero reflectance at a single wavelength, or a multilayer system possessing low reflectance over a wide range of wavelengths. The type used in any particular application depends on a variety of factors, including the substrate material, the wavelengths involved, the film materials available, the required performance and the cost. Both narrowband and wideband multilayer AR coatings on glass substrates were designed and synthesized by ESA in this thesis. As with other thin film fabrication approaches, the ESA technique is limited by the available film materials with special refractive index. Single layer coatings would require film refractive indices of 1.26; no material is available in this range. Another obstacle was the absorbance range of the high-index materials. There is an absorption peak below 550nm for Poly S-119/PDDA. As a result, reflection characteristics at the wavelengths over 550nm were studied, instead of 400-700nm, the visible range.

Narrowband and wideband AR filters are designed and optimized using TRCalc. For narrowband filters, a single optimizing target value is set, i.e., reflectance at the wavelength of 650nm is zero. As for the wideband filter, 11 discrete optimizing target values are set from 600nm to 800nm

with a step of 20nm. Tables 4-4 and 4-5 show the layer structure for the two types of AR filters. In order to precisely control the thickness, the dipping time for the top layer was adjusted according to the fraction portion of the number of the bilayers. The simulation and experiment results for two samples are illustrated in Figures 4-16 to 4-19. Figure 4-20 shows the layer sensitivity for the wideband AR filter. It is clear that the top layer is most sensitive to manufacturing errors.

Table 4-4. Layer structure of narrowband AR filter.

	Layer 1	Layer 2	Layer 3
Material	H*	L*	H
N	1.68	1.54	1.68
QWOT	1.0159	1.0159	2.0321
Thickness (nm)	96.63	105.61	193.30
# of bilayers	34.5	46	69
Optimize	Yes	Yes	Yes

Table 4-5. Layer structure of wideband AR filter.

	Layer 1	Layer 2	Layer 3	Layer 4	Layer 5	Layer 6
Material	H*	L*	H	L	H	L
N	1.68	1.54	1.68	1.54	1.68	1.54
QWOT	0.6024	0.1962	1.1756	1.0719	1.0590	1.0581
Thickness (nm)	58.20	20.72	113.58	113.18	102.31	111.73
# of bilayers	20.8	9	40.6	49.2	36.5	48.6
Optimize	Yes	Yes	Yes	Yes	Yes	Yes

H: PDDA/Poly S-119 L: PDDA/PSS

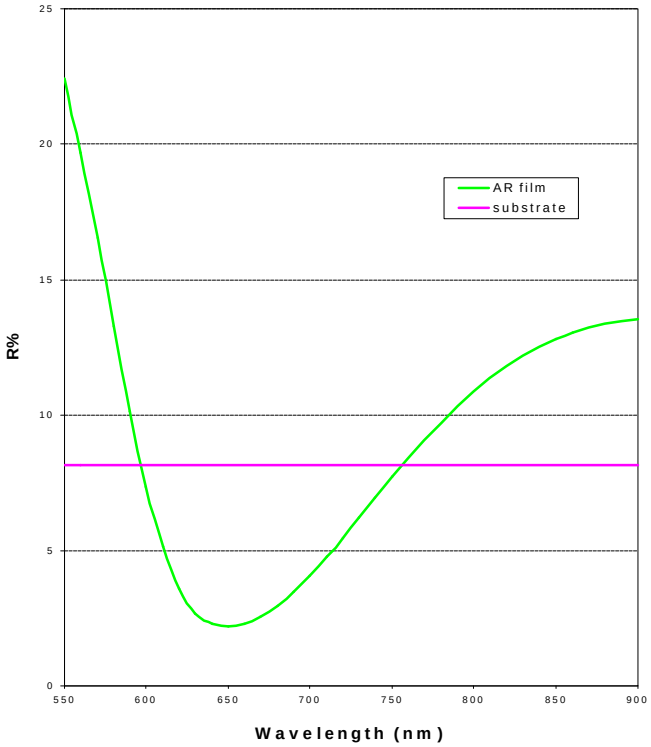

Figure 4-16. Simulated reflectance spectrum of narrowband AR filter.

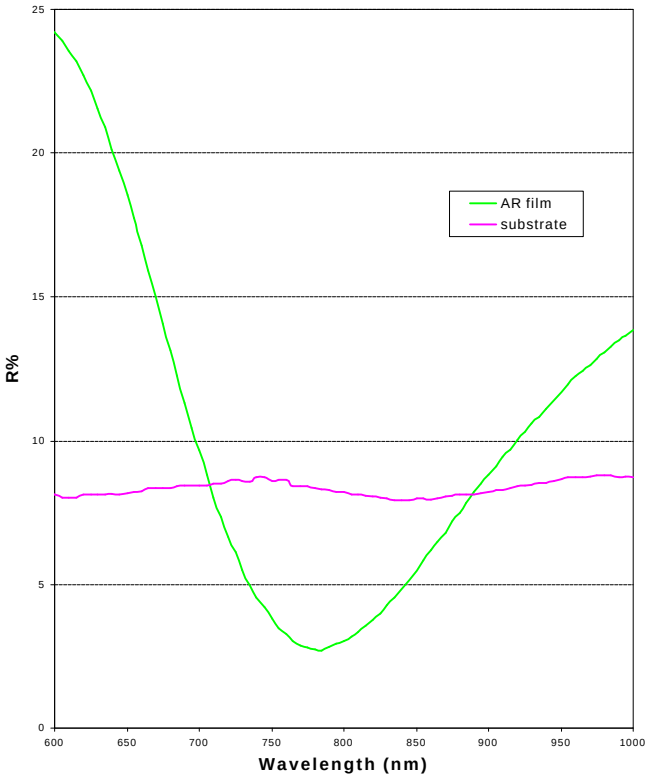

Figure 4-17. Experimental reflectance spectrum of narrowband AR filter.

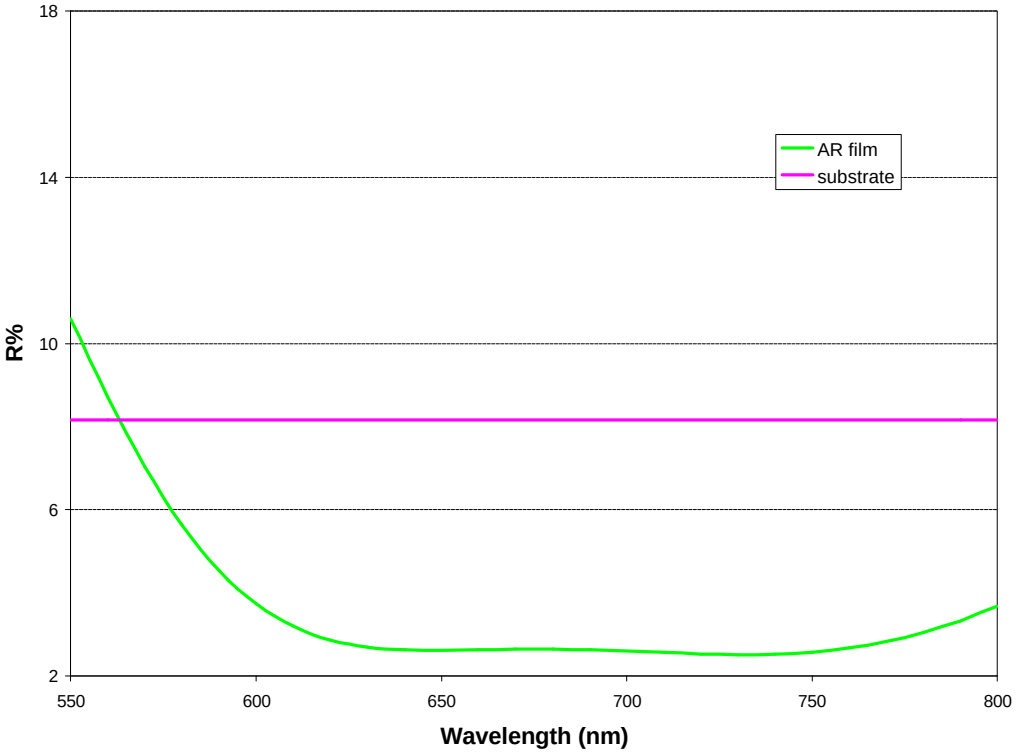

Figure 4-18. Simulated reflectance spectrum of wideband AR filter.

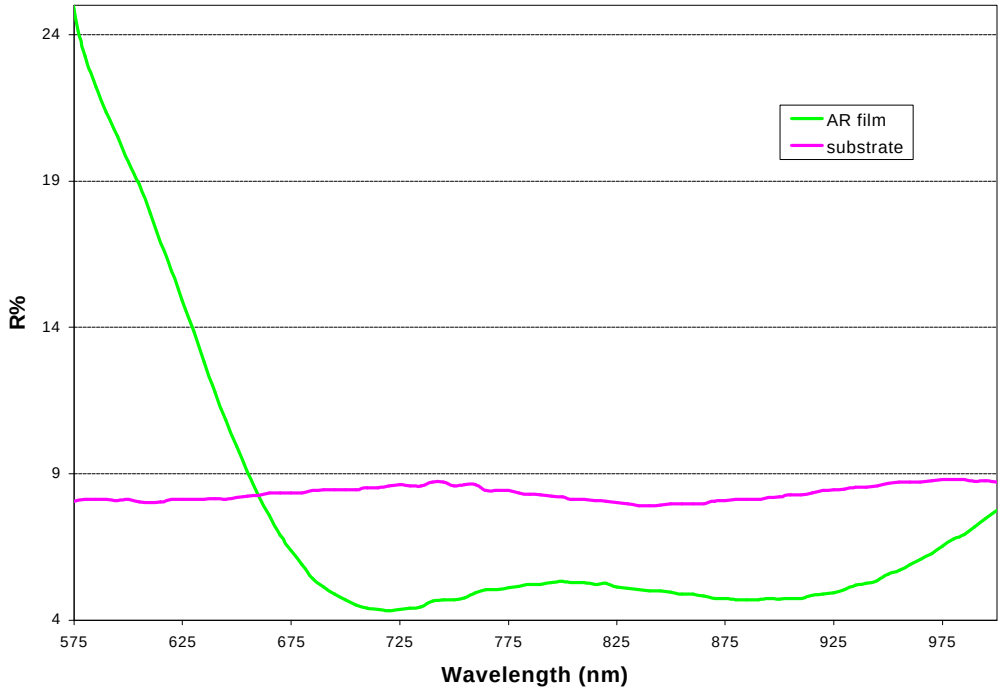

Figure 4-19. Measured reflectance spectrum of wideband AR filter.

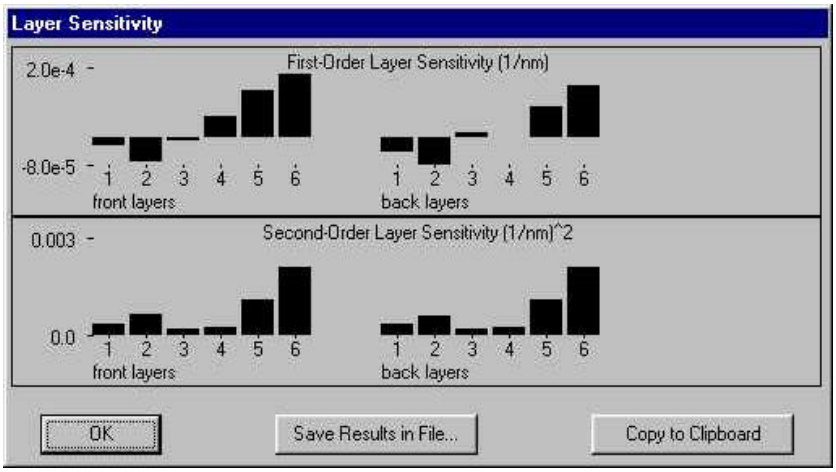

Figure 4-20. Layer sensitivity for the wideband AR filter.

In the above two designs, a fixed refractive index material for each layer is used. The following design employs a material with variable index, which is at the intermediate of the high and low index. The variable index is applied and optimized to the first layer; the thickness of all layers is optimized at the same time with the discrete targets. Table 4-6 shows the optimized layer structure for a wideband AR filter with variable index material. Layer 1 is synthesized using the multilayer patterning index control method discussed before, which consists of 37.1% PDDA/PS-119 and 62.9% PDDA/PSS, corresponding to about 11 bilayers of PDDA/PS-119 and 24 bilayers of PDDA/PSS. The simulation and experiment results for this filter are illustrated in Figures 4-21 and 4-22.

Table 4-6. Layer structure of wideband AR filter with variable index material

	Layer 1	Layer 2	Layer 3
Material	M	H	L
N	1.598	1.68	1.54
Index optimized	Yes	No	No
QWOT	1	1	1
Thickness (nm)	86.04	81.85	89.29
Thickness optimized	Yes	Yes	Yes

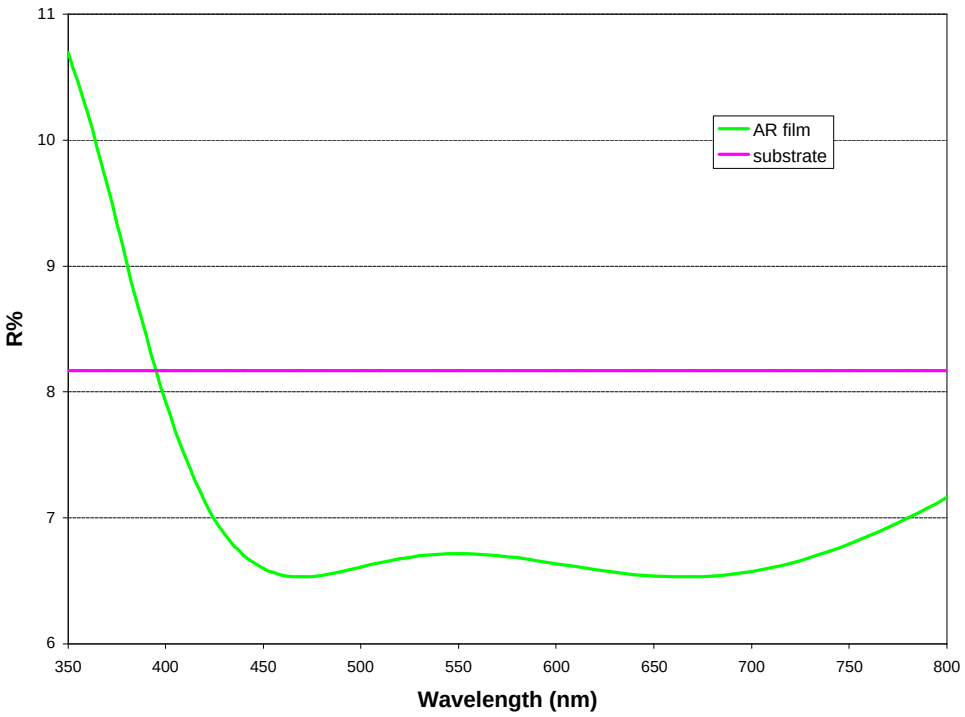

Figure 4-21. Simulated reflectance spectrum of wideband AR filter with variable index material.

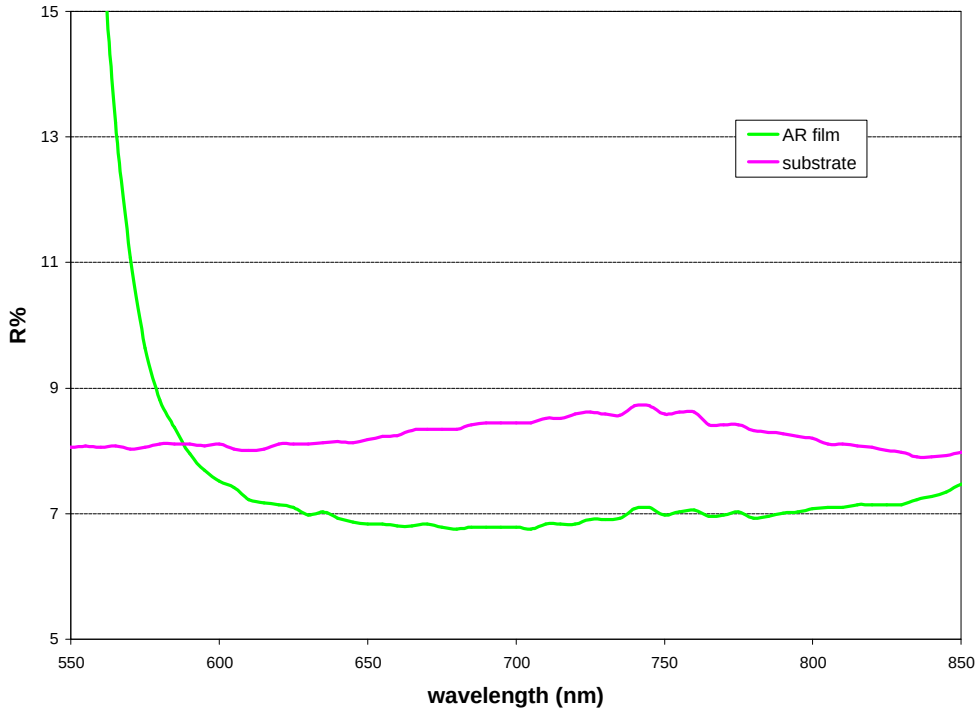

Figure 4-22. Measured reflectance spectrum of wideband AR filter with variable index material.

The above experimental results indicate the feasibility to fabricate the AR filter using ESA method. An approximate agreement between simulation and experiment is shown in the above figures, especially in the reflectance spectra of wideband AR filters. One of the possible reasons for imperfect agreement is the non-uniformity of the substrate. The measured reflectance of the substrate is about 7.91-8.72%, exhibiting a large fluctuation within the range of 600nm to 850nm. To eliminate this fluctuation is the prerequisite of improving the performance of the AR filter. Meanwhile, the AR filter design will be greatly improved by the possibility of water-soluble high index materials with negligible absorbance in the visible wavelengths.

4.4 Summary

Multilayer linear optical interference filters fabricated using ESA processing is investigated in this chapter. Basic single anion/single cation ESA films are fabricated and their optical parameters – refractive index and average thickness for individual bilayers are measured to provide a basis for the design of optical filters. The multilayer patterning method of grading refractive index through the film thickness was discussed.

High performance dielectric stack filters are designed using TFCalc simulation software and are fabricated by ESA. The significant agreement between simulation and experiment demonstrates the strong capability of ESA to precisely control the refractive index and produce excellent thin film filters. The performance of the dielectric stack filters is largely enhanced compared to the results of previous work. In addition, multilayer narrowband and wideband antireflection coatings are designed and fabricated. Different kinds of optimization are employed during simulation until a desired structure is reached. Film sensitivity to manufacturing errors and layer sensitivity are calculated. The experimental results indicate that the ESA process is an excellent choice to fabricate optical filters and other optical structures that require precise index profile control.

4.5 References

7. J.A. Dobrowolski, "Usual and Unusual Applications of Optical Thin Films - An Introduction," in *Handbook of Optical Properties Vol. 1: Thin Films for Optical Coatings*, ed. R.E. Hummel and K.H. Guenther, CRC Press, Boca Raton (1995).
8. R.E. Hummel, K.H. Guenther, *Handbook of Optical Properties*, CRC Press, Boca Raton (1995).
9. F.R. Flory, *Thin Films for Optical Systems*, M. Dekker, New York (1995).
10. J.D. Rancourt, *Optical Thin Films User Handbook*, SPIE Optical Engineering Press, Bellingham, Washington (1996).
11. Y. Liu, *Characterization and Patterned Polymer Films from a Novel Self-Assembly Process*, Ph.D. dissertation, Chemistry Department, Virginia Polytechnic Institute & State University, May 1996.
5. K. Cooper, "Electrostatic Self-Assembly of Linear and Nonlinear Optical Thin Films", Ph.D. dissertation, Electrical Engineering Department, Virginia Polytechnic Institute & State University, Blacksburg, Virginia, May 1996.
7. H.A. Macleod, "Optical thin film coating design," *Proc. SPIE* Vol. 2776, p. 2 (1996).
8. C. Amra, A. Macleod, *Advances in Optical Interference Coatings*, *SPIE* Vol. 3738, Bellingham, Washington (1999).

Chapter 5 *Conclusion*

The Electrostatic Self-Assembly (ESA) process involves alternate adsorption of oppositely charged polyions from aqueous solutions. Extremely uniform films can be deposited on substrates of arbitrary size and shape through the ionic bonding between molecules, allowing nanoscale control over the film thickness and refractive index. Almost any substrate material can be employed using ESA, since no heating or high pressure is required by ESA synthesis. The incorporation of a wide range of inorganic and organic molecules enables the molecular-level control of coating electronic, conductive, optical, magnetic, thermal and mechanical properties. ESA films have high resistance to chemical and environmental effects and the whole synthesis system is inexpensive.

Possessing so many great advantages over traditional thin film fabrication methods, the ESA technique may be widely applied to the fields of optics, electronics, sensing and surface coatings. This thesis demonstrates the feasibility of fabricating linear optical interference filters by ESA methods. The film's bulk optical, electronic, magnetic, thermal, mechanical and other properties are determined by the selection of the molecules in each layer, their orientation at the molecular level, and the order and the thickness of each layer are assembled. Basic single-anion/single-cation ESA films are synthesized and their optical properties are studied to provide a basis for the in-depth design of optical filters. The multilayer patterning method is investigated to allow grading refractive index through the film thickness.

Two types of linear optical interference filter, dielectric stack filters and antireflection coatings, including narrowband and wideband AR coatings, are designed and optimized using TFCalc

simulation software and then fabricated by ESA method. Both bulk film sensitivity and layer sensitivity to manufacturing errors are provided. The significant agreement between simulation and experiment demonstrates the feasibility of synthesis of both step and graded index structures and the strong capability of nanoscale control over film optical properties. The performance of optical thin film filters is greatly enhanced compared to the results of previous methods. The experimental results indicate that ESA process is ready to fabricate linear optical interference filters and other optical structures that require precise index profile control.

The experimental results also show that the reflectance property of the substrate is not uniform within the wavelength range of 600nm to 850nm, which produces a poor filter response. How to eliminate the reflectance fluctuation is future work. In addition, water-soluble materials with higher index (>1.68) and lower index (<1.54) with negligible absorption in the visible wavelength range are required to acquire wider range and higher transmission AR filters. The search for such kinds of materials is underway. Another thing should be indicated here is that all of the simulations and experiments were performed and measured in the case of the normal incidence. It would be a valuable thing to analyze the effect of the non-normal incidence to see how to make the thin films act in the same or similar way no matter from which direction the incident light comes, which is useful when ESA thin film is applied to the eye-glasses.

VITA

Zhaoju Luo

Zhaoju Luo was born on July 22, 1973 in Sichuan Province, China. In 1990 she entered Tsinghua University, and got her Bachelor of Science and Master of Science degree in Electrical Engineering in 1995 and 1998, respectively. Zhaoju achieved good performance in academic works and was awarded “Excellent Student” scholarship each year.

In 1998 Zhaoju joined the Fiber & Electro-Optic Research Center (FEORC) of Virginia Polytechnic Institute and State University as a graduate research assistant in areas of software design and both opto-electronic and signal processing hardware design. She has been involved in several projects funded by the Navy, DARPA and the air force, as well as some small high tech companies.